JGR Atmospheres

RESEARCH ARTICLE
10.1029/2024JD042905

Mountain-Facilitated Lee-Slope Transport and Daytime Boundary Layer Mixing of Volcano Plumes Exacerbates Air Pollution Over Arequipa, Peru

Xiao-Ming Hu[1,2], Ming Xue[1,2], Tingting Qian[3], Xingliang Li[4], Hector Mayol Novoa[5], Jose Luis Ticona Jara[6], Lan Gao[2], Elinor Martin[2], Yongjie Huang[1], and Adriana E. Larrea Valdivia[5]

[1]Center for Analysis and Prediction of Storms, University of Oklahoma, Norman, OK, USA, [2]School of Meteorology, University of Oklahoma, Norman, OK, USA, [3]State Key Laboratory of Severe Weather / Institute of Tibetan Plateau Meteorology, Chinese Academy of Meteorological Sciences, Beijing, China, [4]Earth System Modeling and Prediction Center, China Meteorological Administration, Beijing, China, [5]Universidad Nacional de San Agustín de Arequipa, Arequipa, Perú, [6]Servicio Nacional de Meteorología e Hidrología del Perú (SENAMHI), Arequipa, Perú

Key Points:

- Plumes from volcano Sabancaya can be transported to Arequipa through a series of advection and dispersion processes, thus exacerbating air pollution
- Sabancaya plumes can be captured by Mountain Chachani and transported to Arequipa by nighttime downslope winds linked to gravity waves
- Daytime convective boundary layer entrainment and dispersion further brings elevated plume over Arequipa to the surface

Correspondence to:

X.-M. Hu, M. Xue and H. M. Novoa,
xhu@ou.edu;
mxue@ou.edu;
hnovoa@unsa.edu.pe

Citation:

Hu, X.-M., Xue, M., Qian, T., Li, X., Novoa, H. M., Ticona Jara, J. L., et al. (2025). Mountain-facilitated lee-slope transport and daytime boundary layer mixing of volcano plumes exacerbates air pollution over Arequipa, Peru. *Journal of Geophysical Research: Atmospheres*, *130*, e2024JD042905. https://doi.org/10.1029/2024JD042905

Received 6 NOV 2024
Accepted 25 FEB 2025

Abstract Severe air pollution plagues Arequipa, Peru, due to anthropogenic and natural emissions. Persistent volcano emission in the vicinity of Arequipa makes it among the largest SO_2 sources in the world. Because volcano plumes mostly exist in the free troposphere and stratosphere where horizontal transport acts rather quickly, previous studies mostly focused on their global-scale impacts. Whether these plumes can affect near-surface air quality has not attracted much research attention. This study uses WRF-Chem simulations to reveal that in the presence of northerly/northwesterly winds and favorable mountain meteorology, the plume from volcano Sabancaya (elevation 5,960 m, ~80 km north of Arequipa) can be brought down to near the surface of Arequipa through two steps of transport and dispersion processes: (a) With northerly/northwesterly winds, the free troposphere plume from Sabancaya is transported southward and intercepted by Mountain Chachani located between Sabancaya and Arequipa and subsequently transported downward to Arequipa by nighttime downslope winds linked to large-amplitude lee-side mountain gravity waves. Often the plume reaches down to be close to the boundary layer over Arequipa. (b) In the following day, convective boundary layer growth brings the above boundary-layer plume to near the surface through vertical mixing processes, thus exacerbating ambient air pollution in Arequipa. A mechanism on how volcano plumes above 6-km height cause air pollution over the lower-lying Arequipa city is therefore revealed for the first time. The mountain dynamic effect in inducing the large-amplitude mountain lee waves is further illustrated by an idealized simulation excluding mountain's thermal effect.

Plain Language Summary Severe air pollution often plagues Arequipa, Peru. However, its air pollution formation mechanisms and contributing factors in the region are barely examined. Persistent gas emission from volcanoes in the surrounding region makes the region one among the largest SO_2 sources in the world. Given the high elevation of the volcano vent, it is not clear if the emitted gas plumes can reach the ground level to affect air quality there. Numerical model simulations performed in this study reveal how under favorable meteorological conditions the SO_2 plume released from volcano Sabancaya that is located 80 km north of Arequipa is brought down to the low-lying Arequipa city. When the prevailing winds blow from the north/northwest, the SO_2 plumes from Sabancaya are transported southward to encounter Mount Chachani. At night, the SO_2-carrying stable flow descends along the lee slope of Mount Chachani, in the form of downslope winds in response to the mountain-forced gravity waves. During daytime, the SO_2 plume transported to over the boundary layer of Arequipa are further mixed downward to the surface by boundary-layer eddies forced by surface heating, causing air pollution in Arequipa.

1. Introduction

Severe air pollution plagues several regions over South America, including the Arequipa city beside Andes in southern Peru due to anthropogenic emissions, volcanoes, wildfires, dust emissions, and poor air quality management (Carbo-Bustinza et al., 2022; Cazorla et al., 2022; Colla et al., 2021; Feron et al., 2023; Gómez Peláez et al., 2020; Jury & Gaviria Pabón, 2021; Larrea Valdivia et al., 2020; Li, Michalski, et al., 2021; Michalski et al., 2022; Nawaz & Henze, 2020; Olson et al., 2021; Silva et al., 2018; Yamasoe et al., 2015) with the

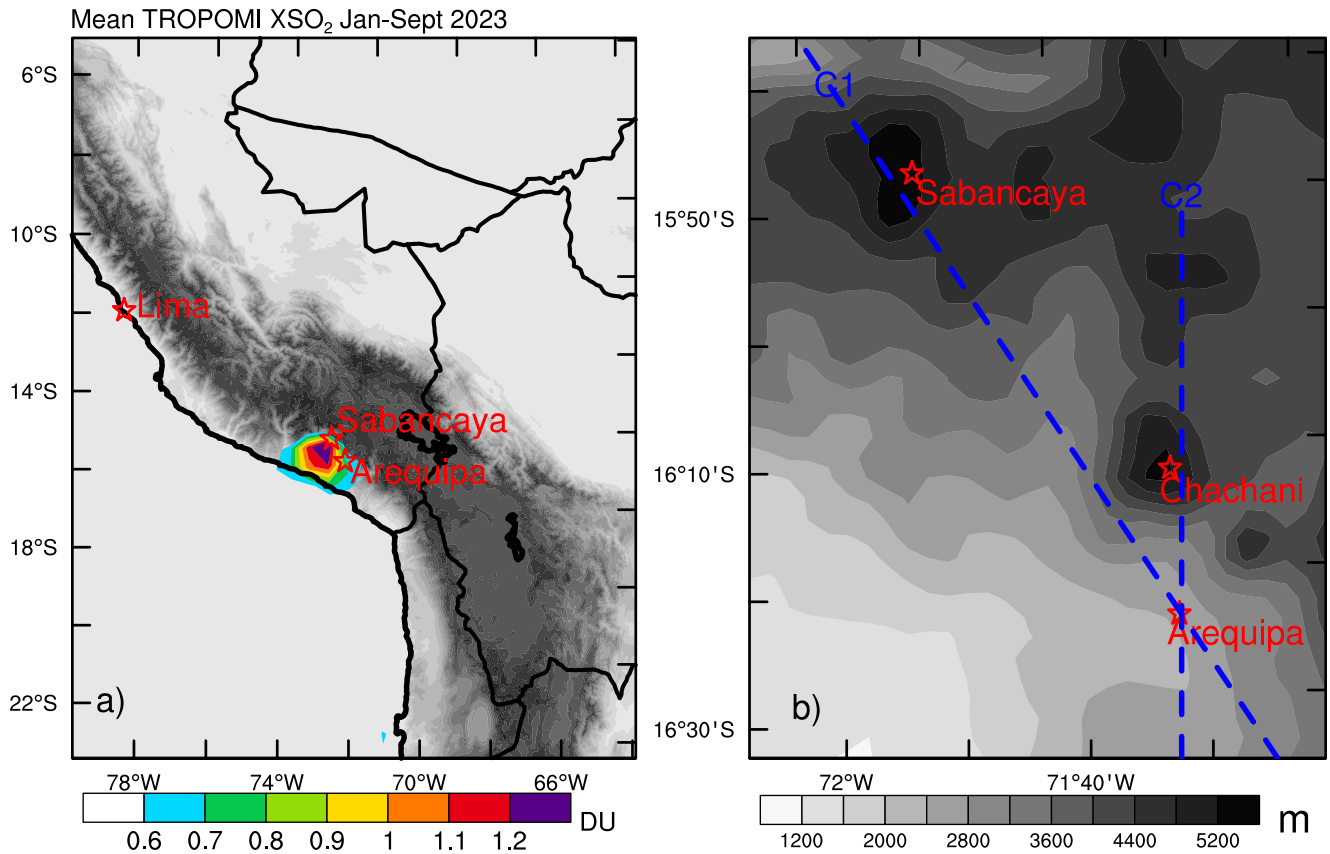

Figure 1. (a) Average column-integrated SO_2 (XSO_2) during January–September 2023 from TROPOMI overlaid on terrain height in domain 2 of WRF-Chem simulations and (b) detailed terrain height around Arequipa, Peru. Location of cross-sections (C1 and C2) are marked.

amplification effects of the meteorological processes in this mountainous region. Particulate matter (PM or aerosols), sulfur dioxide (SO_2), mercury, carbon monoxide (CO), nitrogen oxides (NOx), and ozone (O_3) are the major air pollutants in the Arequipa region. PM with a diameter ≤2.5 μm ($PM_{2.5}$) poses severe health risks. High $PM_{2.5}$ is also believed to exacerbate the transmission and geographic spread of virus-driven infectious diseases. Vasquez-Apestegui et al. (2021) attributed the high rates of COVID-19 cases in Peru to the increased $PM_{2.5}$ exposure during the pandemic years, among other reasons. $PM_{2.5}$ concentration in Arequipa frequently exceeds 200 μg m^{-3} (Larrea Valdivia et al., 2020), with sulfate (SO_4^{2-}), nitrate (NO_3^-), and carbonate aerosols being the major components (Olson et al., 2021). Fossil fuel combustion and dust are previously presumed to be the major sources of $PM_{2.5}$ over Peru, and other contributing sources remain to be identified (Huamán De La Cruz et al., 2019; Olson et al., 2021; Pearce et al., 2009; Valdivia-Silva et al., 2009). Unique local mining activities and volcano emissions likely exacerbate air pollution over Arequipa (Moussallam et al., 2017; Nriagu, 1994; Torres & De-la-Torre, 2022).

SO_2, a precursor of sulfate, shows elevated column-integrated concentration (referred to as XSO_2) over southern Peru (Figure 1a), which may partially contribute to the aerosol pollution in the region through oxidization and the subsequent gas-particle mass transfer process if the near-surface SO_2 is appreciable (Graf et al., 1997; Hu et al., 2008; von Glasow et al., 2009). The Arequipa region is ranked among the top sources of SO_2 pollution in the world because of the two active volcanoes emitting significant amount of gases in the vicinity (Fioletov et al., 2016), that is, volcanoes Ubinas (70 km to the east) and Sabancaya (80 km to the north, see Figure 1b for the location). Volcanoes Ubinas and Sabancaya are among the top volcanic emitters in the world, contributing nearly 1 M tons/year of SO_2 and CO_2 (Burton et al., 2013; Carn et al., 2017; Moussallam et al., 2017). The total volcanic SO_2 emission from Ubinas and Sabancaya is dominated by persistent daily degassing rather than the occasionally explosive eruptions (Moussallam et al., 2017; Shinohara, 2008, 2013). In recent years, Sabancaya is more active than Ubinas, emitting more prominent SO_2 plumes (Figure 1a).

Because the volcano plumes from explosive eruptions mostly exist in the free troposphere and stratosphere where horizontal transport acts rather quickly and influence continental to global scale, previous studies mostly focused on global-scale impacts of volcano plumes, for example, on climate (Dutton & Christy, 1992; Free & Robock, 1999; Gao et al., 2021; Gregori, 1995; Hegerl et al., 2003; Kirchner & Graf, 1995; Mann et al., 1998; Marshall et al., 2022; McCormick et al., 1995; Raible et al., 2016; Schurer et al., 2013; Tett et al., 1999). Previous research of the impacts of volcano plumes on near-surface air quality is limited to a few low elevation volcanoes, including Kilauea (elevation 1,250 m above sea level) in Hawaii (Crawford et al., 2021; Holland et al., 2020; Tang et al., 2020; Whitty et al., 2020), volcano LUSI (elevation 700 m) of Indonesia (Hidayati et al., 2018), Miyake (elevation 775 m) of Japan (An et al., 2003), Cumbre Vieja (elevation 1,949 m) of Spain (Filonchyk et al., 2022). A model trajectory study suggests that volcano plumes injected to the upper troposphere (>5 km above sea level) barely impact surface air quality for a few European volcanoes (Thomas et al., 2017).

Sabancaya (15.787°S, 71.857°W; summit elevation 5,960 m) has been closely monitored by the Instituto Geológico Minero y Metalúrgico (INGEMMET), a Peruvian scientific and management agency. It is characterized by daily explosions or degassing with high SO_2 emission since 2016 (Global Volcanism Program, 2022). The volcano plumes rise 800–4,000 m above the summit and drift in the free troposphere. Daily volcano SO_2 emissions vary significantly, ranging from 400 to 5,600 tons/day (Global Volcanism Program, 2022), and Moussallam et al. (2017) estimated the Sabancaya emission rate to be 2,313 ± 529 tons/day. Some light ashfall is reported around the volcano during recent years, but rarely reaches Arequipa that is ∼80 km to the south, likely due to the substantial deposition rate of particles that limited the particle transport distance (Global Volcanism Program, 2022). However, whether the volcano gas plumes with rich SO_2 can reach near the surface over Arequipa and exacerbate the ambient air quality remains unknown.

While there has been some observational studies of air pollution in Arequipa (e.g., Larrea Valdivia et al., 2020; Olson et al., 2021), the air pollution formation mechanisms and contributing factors (e.g., favorable meteorological conditions) have been little examined using modeling tools in the region. Arequipa is located within the Chili River valley in the Central Andes region with the Pacific Ocean to the west and the Andes Highland to the east and northeast (Figure 1a). Mountain Chachani (summit elevation of 6,057 m) and volcano Sabancaya are 20 and 80 km to the north (Figure 1b). In this mountainous region, topography plays an important role in modulating local meteorological processes and air quality through dynamic and thermal effects (Chow et al., 2012; Richner & Hächler, 2013; Sandu et al., 2019). Dynamic effects refer to topography's blocking effect to divert flows through its physical presence (Jackson et al., 2013), while thermal effects refer to the buoyancy effects associated with heating/cooling of topography and subsequently the lower atmospheric layers (Zardi & Whiteman, 2013). The related meteorological processes include thermally driven mountain-plain solenoids (Bao et al., 2011; Hu et al., 2014; Qian et al., 2015), mountain gravity waves (Durran, 1986; Xue & Thorpe, 1991), mountain wave breaking (Epifanio & Qian, 2008), hydraulic jump (Baines, 1998), barrier jets (Colle et al., 2002; Doyle, 1997; Emery et al., 2015; Harden et al., 2011; Holt, 1996; Li & Chen, 1998; Loescher et al., 2006; Olson & Colle, 2009; Olson et al., 2007; Overland & Bond, 1993, 1995; Parish, 1983; Schwerdtfeger, 1975), and upstream blocking (Epifanio & Rotunno, 2005). There has been increased concern about topographic effects on atmospheric pollutant transport and air quality in recent environmental and meteorological studies (Hu et al., 2014, 2016; Li, Miao, et al., 2021; Li et al., 2015; Lu et al., 2022; Zhang et al., 2018, 2019).

In this study, model simulations using the weather research and forecasting model with chemistry (WRF-Chem, Fast et al., 2006; Grell et al., 2005; Skamarock & Klemp, 2008) are conducted in the Arequipa region for the first time to reveal that in the presence of favorable meteorological conditions and with Mountain Chachani located 20 km north of Arequipa, the plumes from volcano Sabancaya can be brought to near the surface of Arequipa through a series of atmospheric processes, exacerbating urban air pollution. This study discovers an air pollution formation mechanism over Arequipa focusing on SO_2 as a first attempt.

The rest of this paper is organized as follows: In Section 2, satellite SO_2 and sounding data, WRF-Chem model configurations, and idealized numerical experiment design are described. In Section 3, the pathway of Sabancaya SO_2 plume transported to the surface of Arequipa, thus affecting ambient air quality, is elucidated using these observations and simulations. The importance of the dynamic effect of Mountain Chachani in such a transport pathway is emphasized. Finally, Section 4 contains a summary and discussion of the main findings.

2. Data Process, Model Configuration, and Numerical Experiment Design

2.1. TROPOMI SO_2 Data and Soundings

In Arequipa, in situ air pollutant measurements are deficient (de Moura & da Silva Júnior, 2023; Riojas-Rodríguez et al., 2016). To our best knowledge, currently no in situ SO_2 measurements are being made in Arequipa. Thus, satellite remote sensing data are first explored to understand the large-scale distributions of pollutants in the region. The TROPOMI instrument onboard the European Space Agency's Sentinel-5 Precursor (S5P) satellite has proven to be a valuable tool for studying SO_2 emissions and their distribution, particularly in the context of volcanic eruptions (Fioletov et al., 2020; Koukouli et al., 2022; Markus et al., 2023). TROPOMI is a hyperspectral spectrometer that images atmosphere with 13:30 local time (LT) overpasses, providing a nadir spatial resolution of 3.6 km × 5.6 km and covering a swath width of approximately 2,600 km (Theys et al., 2022). TROPOMI SO_2 product is highly sensitive to SO_2 at high altitudes, and the sensitivity to SO_2 in the lower boundary layer is somewhat limited due to contamination of aerosol, clouds, and ozone absorption.

Following the literature, we used TROPOMI SO_2 data to initially identify large-scale SO_2 patterns resulting from volcanic eruptions. In such cases, enhanced measurement sensitivity for SO_2 in the free troposphere is generally expected from TROPOMI. Specifically, we utilized the SO_2 vertical column densities (VCDs) from the Level 2 offline SO_2 product to quantify the concentration of SO_2 molecules within a given atmospheric column per unit area. These VCDs were then converted into Dobson units (DU) using a conversion factor. To ensure data quality, we applied a filtering process based on the retrieval quality assurance (QA) value, removing samples with a QA value less than 0.5. This step accounted for potential contamination in the retrievals stemming from bright surfaces, presence of clouds, and solar geometries. Finally, the QA-controlled SO_2 data were aggregated into 0.5-degree spatial bins for all available samples throughout the year 2023 (from January to September when we started drafting this paper), enabling us to generate the annual mean pattern of SO_2 distribution, as shown in Figure 1a.

Dispersion of air pollutants highly depends on atmospheric flows and stability. Daily sounding has been launched over Arequipa during early mornings (7–8 LT) since September 2022 on most days with certain days missing. Soundings on May 18 and 7 August 2023 are used for model evaluation and examining the stability conditions in these cases while sounding is not available for the case of 30 July 2023 and three cases before September 2022 examined in this study.

2.2. WRF-Chem Simulations

Daily 48 hr WRF-Chem (version 4.3.3) simulations are conducted to examine the transport/dispersion of SO_2 plumes from volcano Sabancaya for the period of October 2021–March 2022 when Sabancaya activities were recorded and reported by Global Volcanism Program (2022) and for the period of May–August 2023 when in situ soundings from Arequipa are available. Volcano plumes from Sabancaya on most days drifted to the southwest (Figure 1). Six cases in which the southeast-drifting flumes appear to have affected air quality over Arequipa are presented in this manuscript; they are those of 19 and 28 October 2021; 17 March 2022; and May 18, July 30, and 7 August 2023 (summarized in Table 1). Our analyses focus on 21–48 hr simulations to avoid the first 21 hr when the model goes through spin-up. Because the volcano SO_2 emissions dominate the SO_2 fields in the region, and background regional-scale SO_2 contributes insubstantially, we focus on the SO_2 plume from the emission of the Sabancaya volcano within the simulation domain in this study. Thus, a longer spin-up as in other chemistry simulations, where a more spun-up initial chemical composition fields are critical for the subsequent chemical reactions and fields, is unnecessary in this study. The initial and boundary conditions for meteorology are from hourly NCEP FNL (Final) operational global analysis and forecast (GFS) data on the 0.25 × 0.25° grid (National Centers for Environmental Prediction, 2015) and those for chemistry are from the Whole Atmosphere Community Climate Model (WACCM) outputs with a resolution of 0.9 × 1.25° (Gettelman et al., 2019). Two one-way nested domains are run simultaneously with 15- and 3-km horizontal grid spacings covering the entire South America and the Peruvian Central Andes region centered around Arequipa, respectively (see Figure 1 for domain 2 coverage and Figure 1a of Hu et al. (2023) for the exact domain configuration), following our previous convection-permitting regional climate simulations (Hu et al., 2023; Huang et al., 2023, 2024). Both domains use 48 vertical levels extending from the surface to 100 hPa. Physics parameterizations include the Yonsei University (YSU) PBL scheme (Hong et al., 2006), revised MM5 Monin-Obukhov surface layer scheme (Jiménez et al., 2012), and the rapid radiative transfer model for GCMs (RRTMG) longwave and shortwave radiation

Table 1
Summary of Characteristics of Meteorology and SO_2 Plumes During the Six Cases Examined in This Study

Cases	Characteristics
19 October 2021	Prevailing northwesterly winds in the lower troposphere
28 October 2021	Prevailing northwesterly winds in the lower troposphere and vertical or overturning isentropes above ~6 km in early morning
17 March 2022	Prevailing northwesterly winds in the troposphere and two clear steps (wave + mixing) for the SO_2 plume to be transported to the surface
18 May 2023	Prevailing northwesterly winds in the troposphere, prominent vertical or overturning isentropes above ~6 km in early morning, and sounding verification available
30 July 2023	Prevailing northwesterly winds in the troposphere, prominent vertical or overturning isentropes above ~6 km in early morning, and SO_2 plume transported to near the surface over Arequipa in the early morning
7 August 2023	Prevailing northwesterly winds in the troposphere, sounding verification available, and two clear steps (wave + mixing) for the SO_2 plume to be transported to the surface

scheme (Iacono et al., 2008). Because all the cases are free of precipitation over the Arequipa region, microphysics and cumulus schemes are less relevant.

The gas-phase chemical reactions are simulated using the Regional Atmospheric Chemistry Mechanism (RACM, Stockwell et al., 1997), which is implemented within WRF-Chem using the Kinetic PreProcessor (KPP, Sandu et al., 2003). Hourly anthropogenic emissions of chemical species come from the REanalysis of the TROpospheric (RETRO) chemical composition inventories. The SO_2 emission rate from Sabancaya is set to 2,000 tons/day, and the emission is vertically evenly distributed in each model layer from the mountain summit to 10 km above sea level based on previous estimations (Global Volcanism Program, 2022; Moussallam et al., 2017). Note these previous estimations of the daily SO_2 emission rate from Sabancaya range from a few hundred to ~5,000 tons/day. Our simulations adopt a medium rate to represent a moderate daily outgassing. This study focuses on gas SO_2. Aerosol reactions/processes are excluded in these WRF-Chem simulations.

To diagnose the overall (dynamic plus thermal) effects of the nearby Mount Chachani on SO_2 plume over Arequipa, a sensitivity simulation removing the terrain of Chachani is conducted for the case of 30 July 2023.

2.3. Idealized Simulation Only Considering Mountain Dynamic Effects

The WRF-Chem simulations considers both dynamic and thermal effects associated with the complex terrains in the region. Additional idealized simulations only considering the dynamic effect of simplified mountain profiles are conducted to help isolate the dynamic effect of the mountain barrier on the lower level flows. Using an idealized approach can help understand the contributions of the most important effects/processes of primary interest (Braun et al., 1999; Hu et al., 2016; Pu & Dickinson, 2014; Saide et al., 2011). In our case, we are most interested in the flow pattern after the airstream passes over the tall Chachani Mountain located to the north-northwest of Arequipa.

The idealized experiments use the advanced regional prediction system (ARPS) model, a comprehensive regional- to storm-scale atmospheric modeling/prediction system (Xue et al., 2000, 2001, 2003), to simulate air flows around an isolated mountain that mimic the Chachani Mountain to some extent. The thermal effect of the mountain is excluded to isolate the dynamic effect.

An isolated asymmetric bell-shaped mountain with a peak height of 4 km is specified in the model that has an east-west half width of 30 km, and a 20- and 8-km half width on the north and the south side of the mountain peak, respectively. The horizontal grid spacing is 1 km, and vertical grid spacing increases from 100 m at the surface to 900 m at the model top located at 20 km height. The model domain is large enough to avoid any lateral boundary effect. The initial state is set close to the early morning sounding data over Arequipa and is characterized by a

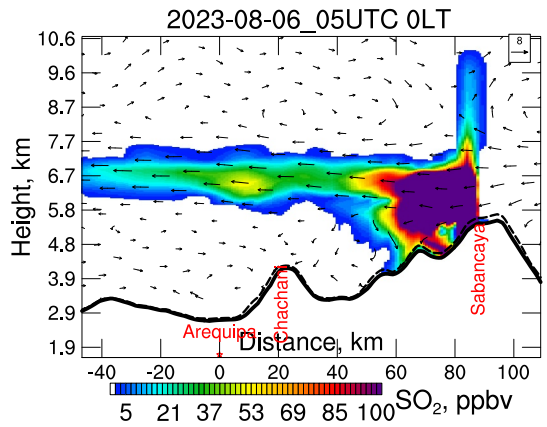

Figure 2. Simulated SO_2 plume from Sabancaya along cross-section C1 (see location in Figure 1b) in the free troposphere on the night of 5–6 August 2023.

constant northerly flow of 7 m s^{-1} and a base state with a constant static stability with a Brunt-Vaisala frequency of $N = 0.01$ s^{-1}. The reference potential temperature (θ) near the surface is 308.5 K. The specified environmental profile and the height of the mountain result in a low Froude number flow. The model simulation is integrated up to 4 hr when the main features of the solution become established.

3. Results

3.1. Climatological SO_2 Plume From Volcano Sabancaya

Volcano Sabancaya (15.787°S, 71.857°W) was active in recent years with persistent daily degassing (Global Volcanism Program, 2022). Such daily degassing was captured by the TROPOMI XSO_2 data. In the TROPOMI average XSO_2 map during January–September 2023, the SO_2 plume with $XSO_2 > 1$ DU around volcano Sabancaya is the only significant source in this Central Andes region (Figure 1a). The average daily total SO_2 abundance in the region amounts to ~4,000 ton. This is consistent with previous reports that the Arequipa region is among the top SO_2 sources in the world (Fioletov et al., 2016, 2020). Given the Sabancaya summit elevation of 5,960 m and its plume rises to 800–4,000 m above the summit (Global Volcanism Program, 2022), the volcano plume is mainly found at 6–10 km above sea level, residing in the free troposphere having a stable stratification. The horizontal winds would normally transport the volcano plume over long distance in the stable free troposphere without much downward transport, often spreading the plume downstream across continent (Filonchyk et al., 2022). Such SO_2 plumes may not be able to affect the air quality near the surface in the Arequipa region that is located in the Chili River valley, if there is no other atmospheric process that brings the plumes down to the surface. Figure 2 shows a typical scenario with the simulated SO_2 plume in the night of August 5–6 mostly found at ~6.7 km above sea level or ~3–4 km above the ground of Arequipa.

3.2. Cases of SO_2 Plumes Using WRF-Chem Simulations

Different from the typical scenario, during periods of October 2021–March 2022 and May–August 2023, we notice some cases with northerly or northwesterly winds, in which the Sabancaya SO_2 plume is brought down to Arequipa's Chili River valley in the WRF-Chem simulations, exacerbating near-surface air quality over Arequipa. Six of these cases are presented in this paper; they are those of 19 and 28 October 2021; 17 March 2022; May 18, July 30, and 7 August 2023 (summarized in Table 1). In these cases, TROPOMI data indicate that XSO_2 plumes emitting from Sabancaya are transported southward and some of the XSO_2 plumes reach as high as 6 DU (Figure 3). Note that TROPOMI XSO_2 data on May 18 are missing while the XSO_2 plumes on May 17 and 19 are prominent. Thus, the southward transported XSO_2 plume on May 19 is shown in Figure 3 instead. Based on the prominent plumes observed on May 17 and 19, we can safely assume there was significant degassing from Sabancaya on May 18 also. The transport pathway of these cases and how they contribute to near-surface air pollution over Arequipa are examined using the simulation data.

For the Sabancaya SO_2 plumes to be transported to Arequipa, northerly or northwesterly large-scale winds are a prerequisite. Using the 7 August 2023 case as an example, in the evening of August 6, an anticyclonic circulation center was located at 64°W, 7°S or to the northeast of Arequipa at the 500-hPa level. The midtropospheric flows over the Arequipa region were northwesterly (Figure 4a). In the morning of August 7, the anticyclone center shifted to about 64°W, and the northwesterly winds on the south side of the anticyclone expanded further south (Figure 4b). Such northwesterly winds favor the southward transport of the volcanic plumes in the free troposphere toward the Arequipa region.

Note that there were clouds over Arequipa on August 6–7, as indicated by the MODIS images (not shown). However, TROPOMI was still able to retrieve the Sabancaya XSO_2 plumes, indicating at least part of the SO_2 plumes was above the clouds, confirming their free troposphere presence. The SO_2 at the high altitudes likely explains the nearly daily detection of prominent Sabancaya XSO_2 plumes by TROPOMI data even though clouds are often present in the region.

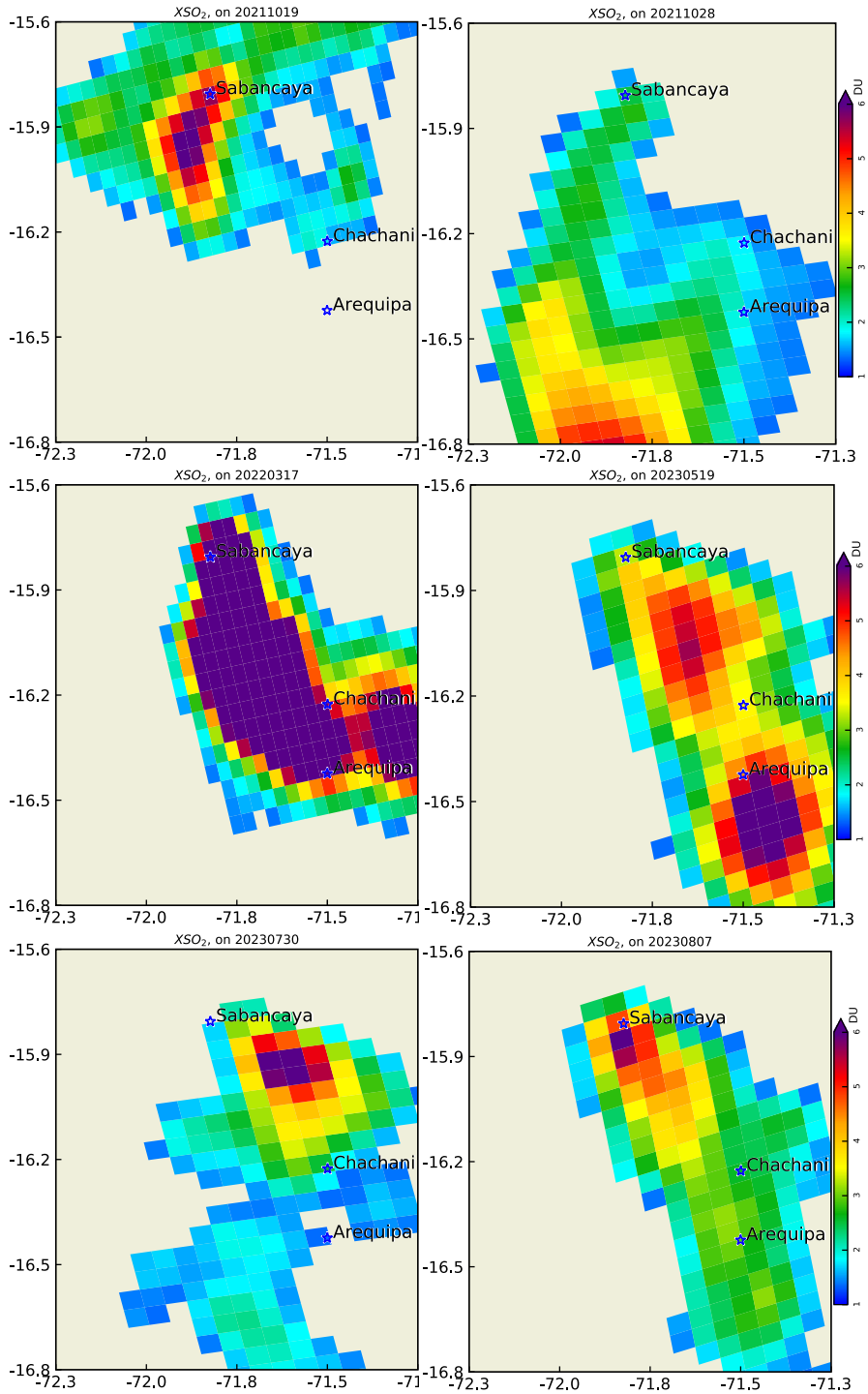

Figure 3. TROPOMI XSO_2 plumes for six cases (i.e., 19, 28 October 2021; 17 March 2022; and May 18, July 30, and 7 August 2023). Note that there is no TROPOMI XSO_2 available on May 18 while the TROPOMI XSO_2 on May 19 shows a prominent plume.

In the presence of northerly or northwesterly large-scale flows, southward-transported midtroposphere Sabancaya SO_2 plumes are intercepted by mountains around Sabancaya including Chachani with a summit elevation of 6,057 m (Figure 5). Note that the elevation of Chachani in the south-north cross-sections in Figure 5 is lower than its summit elevation because these cross-sections through Arequipa do not cut across the summit. In these

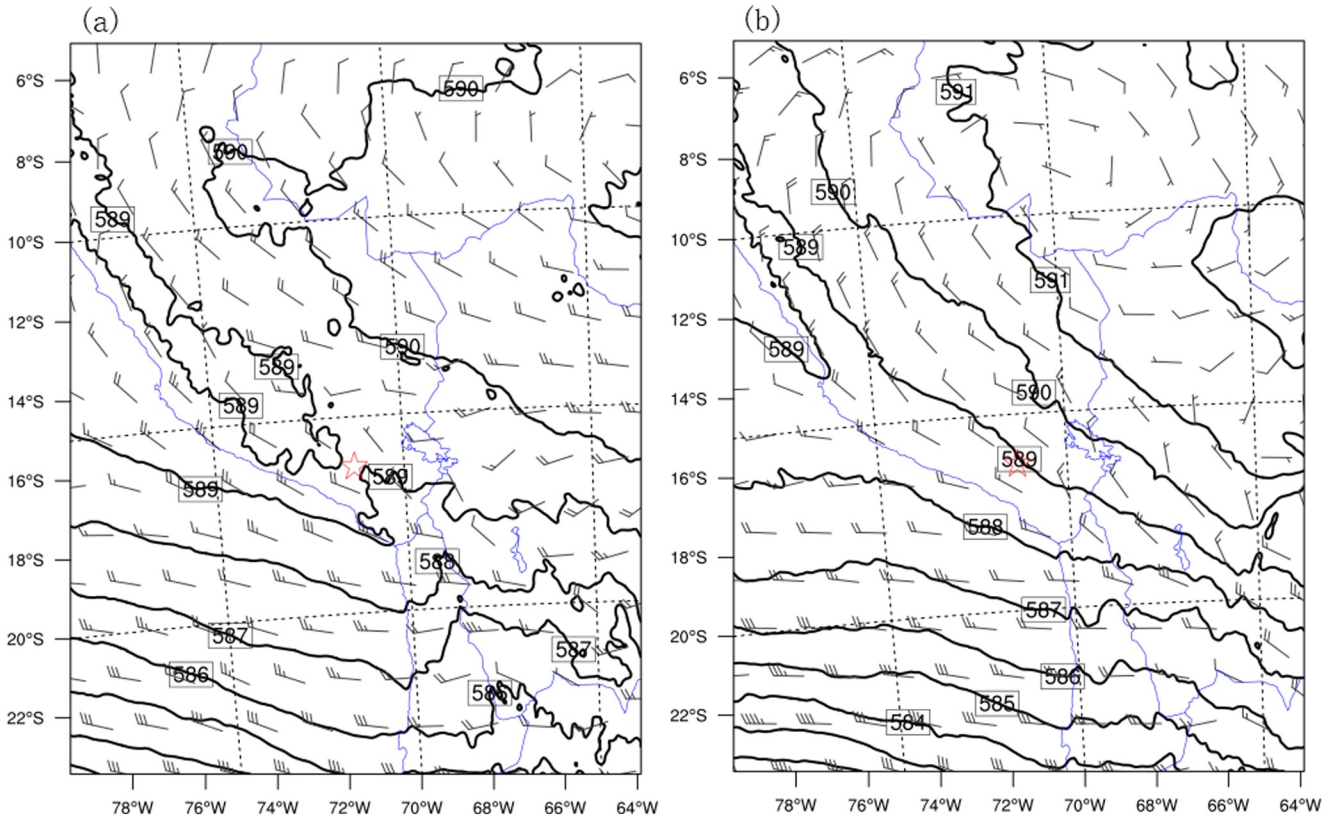

Figure 4. The geopotential height (black solid line, unit: geopotential meter [gpm]) and wind vectors at 500 hPa at (a) 18:00 LT on 2023-08-06 and (b) 04:00 LT on 2023-08-07. The blue thin lines are the country boundaries. The red pentagram is the location of Arequipa.

mountainous regions, daytime convective boundary layer can grow to 1–2 km above the ground, which roughly envelopes the mountain terrain. At some locations, the boundary layer top reaches the level of midtroposphere Sabancaya SO_2 plumes, thus capturing the volcano plumes. Mountain venting processes induced by thermally driven upvalley/upslope flows can further mix pollutants through the boundary layer top, making pollutants well mixed in a deeper layer over mountainous regions (De Wekker et al., 2004; Steyn et al., 2013). At 16 LT of all six cases, the SO_2 plumes are spread over the elevated mountainous region around Sabancaya and intercepted by Chachani (Figure 5). Thus, during the afternoon, the SO_2 concentration is elevated in those high mountainous regions. How does these SO_2-rich mountainous air mass reach low-lying Arequipa at later time is examined in detail below.

During the ensuing nighttime, as nighttime boundary layer develops, stability increases, and potential temperature shows a layered structure around mountains (Figure 6). As the air flows pass over the tall Chachani Mountain, they descend along the downwind slope of the mountain, more or less following the isentropic contours (Figure 7) as the flows are approximately adiabatic. The descending downslope flows act to transport some of the SO_2 plumes to lower levels, toward Arequipa's Chili River valley. The extents of downward transport vary on individual days (Figure 7). On 30 July 2023, the SO_2 plume penetrates to near the surface over Arequipa, while in other cases, the SO_2 plume does not reach the bottom of the valley. This is apparently strongly correlated with static stability of the layer or the potential temperature difference between the mountain top and the valley. On July 30, the difference is only about 6 K (Figures 6e and 7e) while on 17 March 2022, (Figures 6c and 7c), the difference is about 13 K. The much weaker stability on 30 July 2023 allows the downslope flow to reach much lower altitude, as the kinetic energy of the downward flow is converted to potential energy in the stable environment. Eventually, the downslope flow restores to a higher altitude, producing gravity wave oscillations whose signals propagate upward (Figure 7). For these early morning cross-sections, the downslope motion is very likely aided by nighttime drainage flows in lower valleys, enabling the SO_2 plumes to reach lower altitudes than the pure dynamically forced overmountain flow can. We can also see that within the valley near the surface, static stability

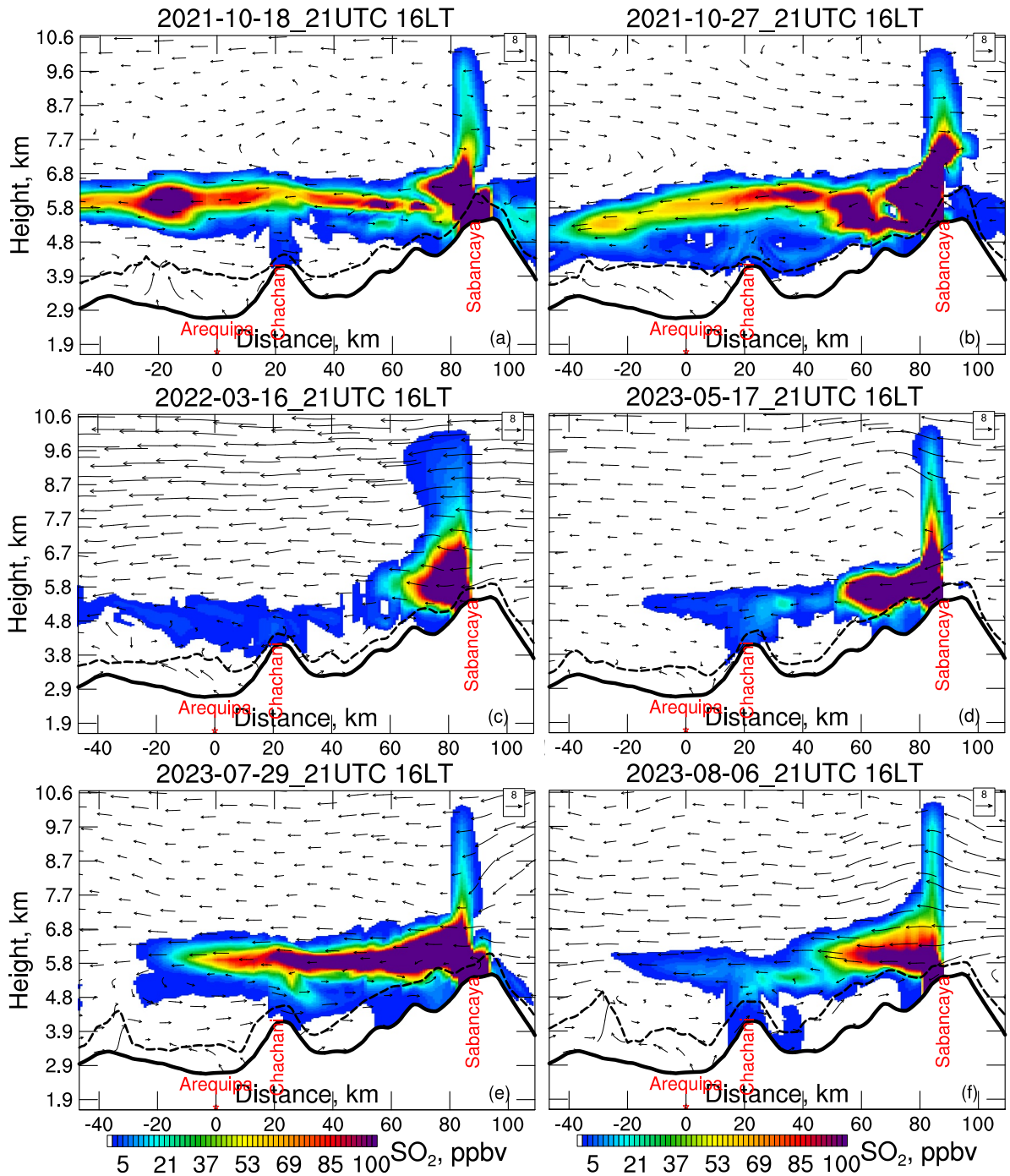

Figure 5. Cross-section of SO_2, and winds through Arequipa and Sabancaya along C1 (see location in Figure 1b) during afternoon on (a) October 18 and (b) 27, 2021; (c) 16 March 2022; and (d) May 17, (e) July 29, and (f) 6 August 2023. The boundary layer top is marked using the black dash lines.

is strong (e.g., Figures 6d, 6f, and 7). Such a stable layer should be the result of nighttime cooling, and will make it difficult for the plumes to penetrate all the way to the ground surface. Figure 8 shows the early morning soundings observed and simulated on May 18 and 7 August 2023 at Arequipa. The simulations reproduce the general boundary layer structures reasonably well, including capturing the early morning near-surface stable layer (Figure 8).

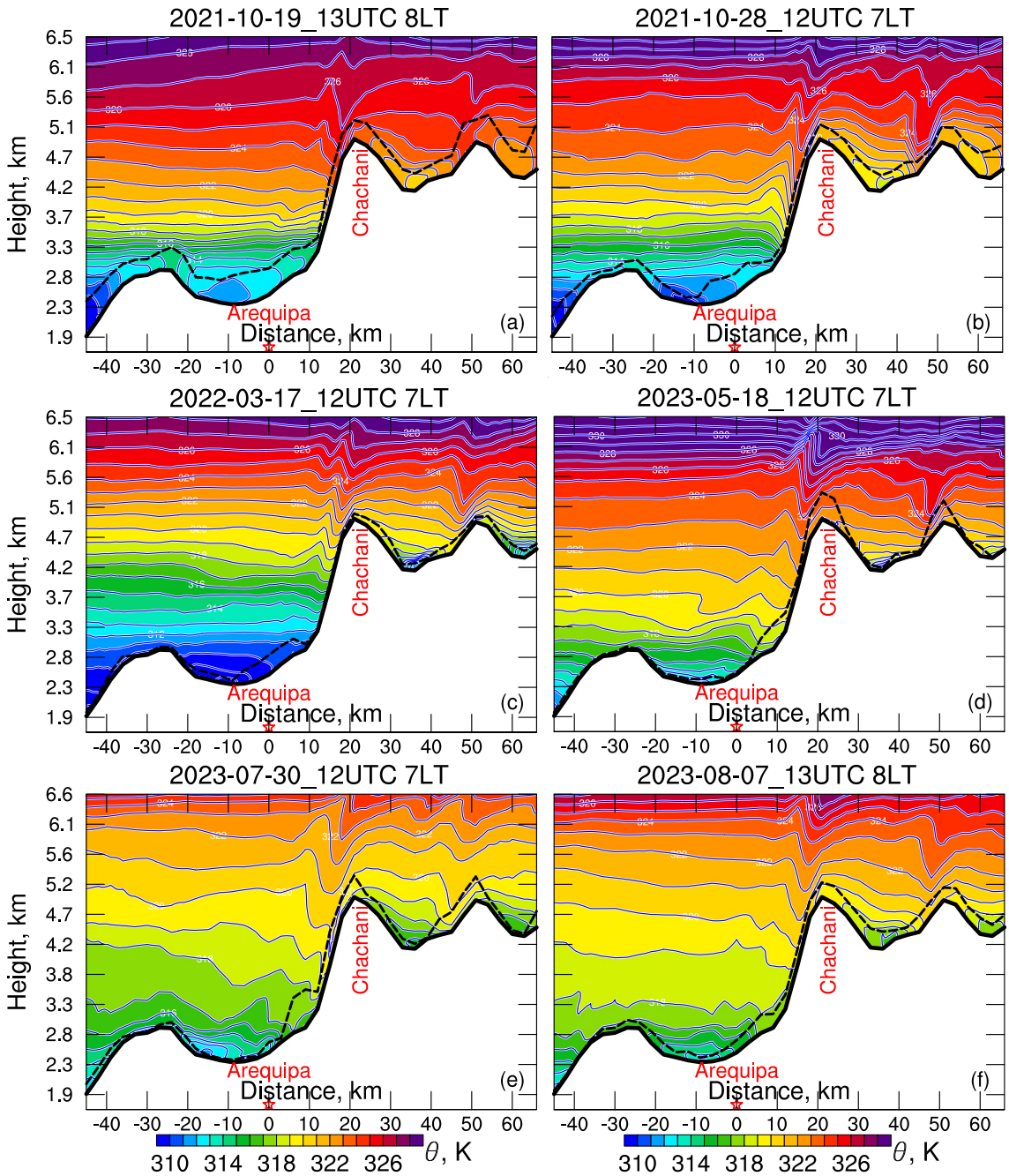

Figure 6. South-north cross-section of potential temperature through Arequipa and Mountain Chachani along C2 (see location in Figure 1b) during early morning on (a) October 19 and (b) 28, 2021; (c) 17 March 2022; and (d) May 18, (e) July 30, and (f) 7 August 2023. The boundary layer top is marked using the black dash lines.

The downward transport of SO_2 plumes on the lee side of Mountain Chachani is examined further in terms of its mechanism. Figure 6 shows the potential temperature contours or isentropes, which can be considered flow streamlines when diabatic heating and turbulent mixing are negligible (Bluestein, 1992; Bonin et al., 2020; Smith, 1979; Xue & Thorpe, 1991). Generally, the atmosphere is stably stratified on the synoptic scale in all six cases as illustrated by the vertical gradient of potential temperature (Figures 6 and 7). Flows over the Chachani Mountain are dominated by the mountain wave pattern above the lee slope during early morning on 19 and 28 October 2021; 17 March 2022; and July 30 and 7 August 2023. The upward propagating gravity waves are of significant amplitudes for these cases, and vertical or overturning isentropes are seen above ~6 km levels on May 18 and July 30 of 2023 (Figures 6d and 6e). When overturning occurs, the stratification becomes unstable and

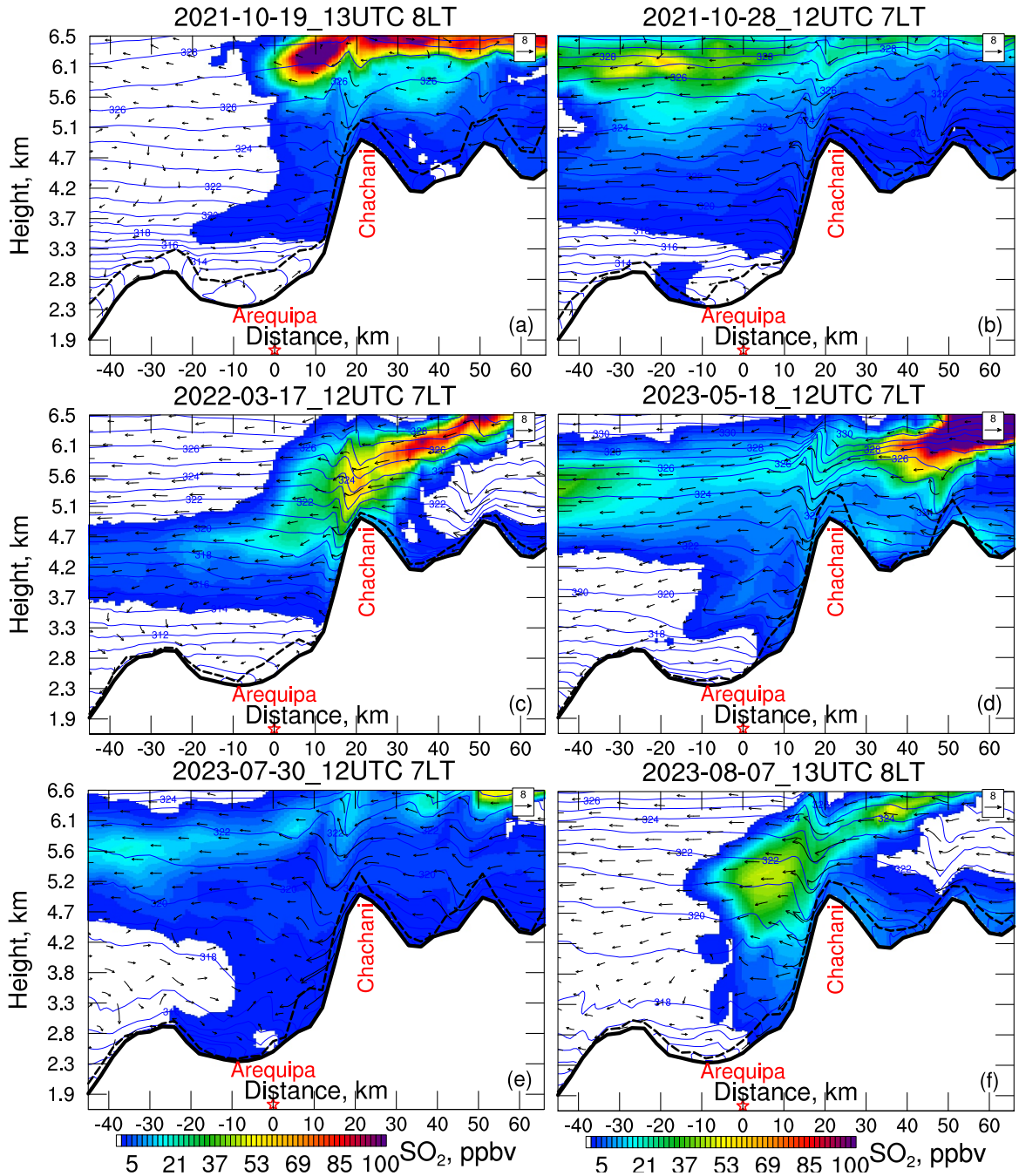

Figure 7. South-north cross-section of SO_2 (shaded), winds (vectors), and potential temperature (contours) through Arequipa and Mountain Chachani along C2 (see location in Figure 1b) during early morning on (a) October 19 and (b) 28, 2021; (c) 17 March 2022; and (d) May 18, (e) July 30, and (f) 7 August 2023. The boundary layer top is marked using the black dash lines.

gravity wave breaking would occur. Peltier and Clark (1979) showed that when wave breaking occurs, the well-mixed layer due to the breaking acts as a critical layer through which gravity waves cannot penetrate, and the downward reflected waves can interfere with upward propagating waves to create enhanced downslope winds on the lee side of the mountain. Such a process would increase the downslope transport of the SO_2 plumes in our case.

These wave features indicate that a mountain's dynamic effect dominates thermal effect under these circumstances. A mountain's thermal effect would lead to colder air near the slope during nighttime and early morning due to radiative cooling (Bao et al., 2011; He & Zhang, 2010; Hu et al., 2014; Qian et al., 2015), which is opposite

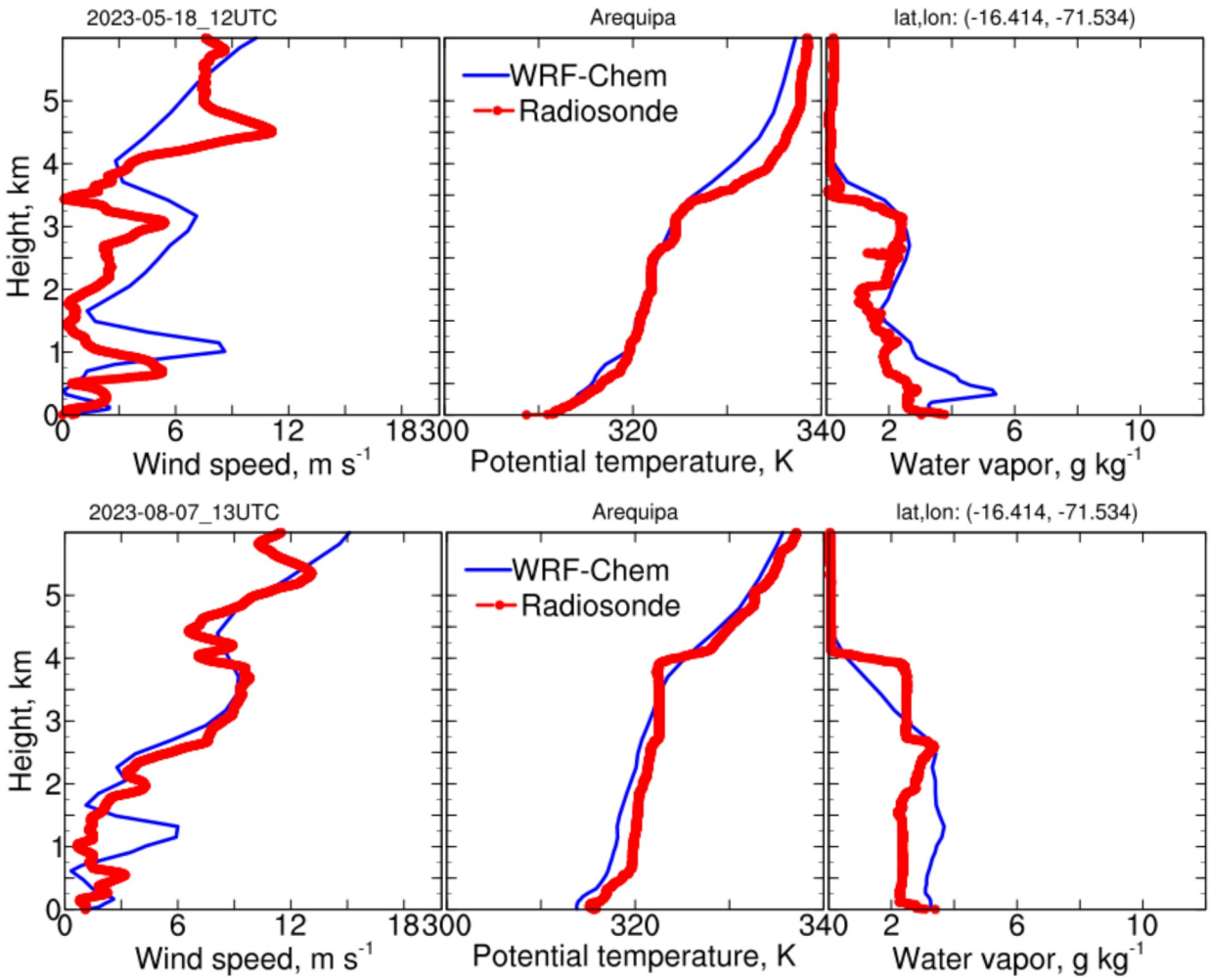

Figure 8. Observed and simulated profiles of (left–right) wind speed, potential temperature, and water vapor mixing ratios over Arequipa during early mornings (7–8 local time) on (top) May 18 and (bottom) 7 August 2023.

to the warm air zone along the upper slope seen in Figure 6. Thus, a mountain's thermal effect must play a minor role in these cases. Air behind the waves accelerates down the slope. The accelerated downslope flows bring the aloft SO_2 downward toward the valley, and the subsequent ascending flows in the wave cause the downstream spread of the SO_2 plumes across the valley (Figure 7). The wave breaking indicated by potential temperature overturns at 7 LT on May 18 and 30 July 2023 (Epifanio & Qian, 2008; Epifanio & Rotunno, 2005) is associated with the accelerated flow near the slope surface and a quick turbulent mixture region above the lee slope, which provides a favorable condition for enhanced SO_2 diffusion downstream for these cases (Figures 7d and 7e).

The vertical movement of air flow in the cross-sections can be illustrated more clearly using the cross-section-normal vorticity component, in this case the y-z plane-normal vorticity $\zeta = \partial w/\partial y - \partial v/\partial z$ (Figure 9). A narrow zone with negative vorticity along the upper part of lee slope is present in all six cases, indicating the downdrafts along the lee slope. The narrow negative vorticity zone, thus downdraft, extends above the Arequipa valley with a positive vorticity zone below, or positive and negative vorticity zones alternating below in some cases, that is, 17 March 2022, and 18 May 2023, indicating reversed circulations over Arequipa (Figure 9). Such reversal circulations and associated turbulence eddies contribute to further downward transport of the downstream SO_2 plumes over Arequipa. However, the altitudes of the reversal layer are different, likely dictated by atmospheric stratification. As a result, the extents of the downward penetration of the SO_2 plumes are different for each case, with the SO_2 plume on 30 July 2023, penetrating to near the surface over Arequipa, and the early

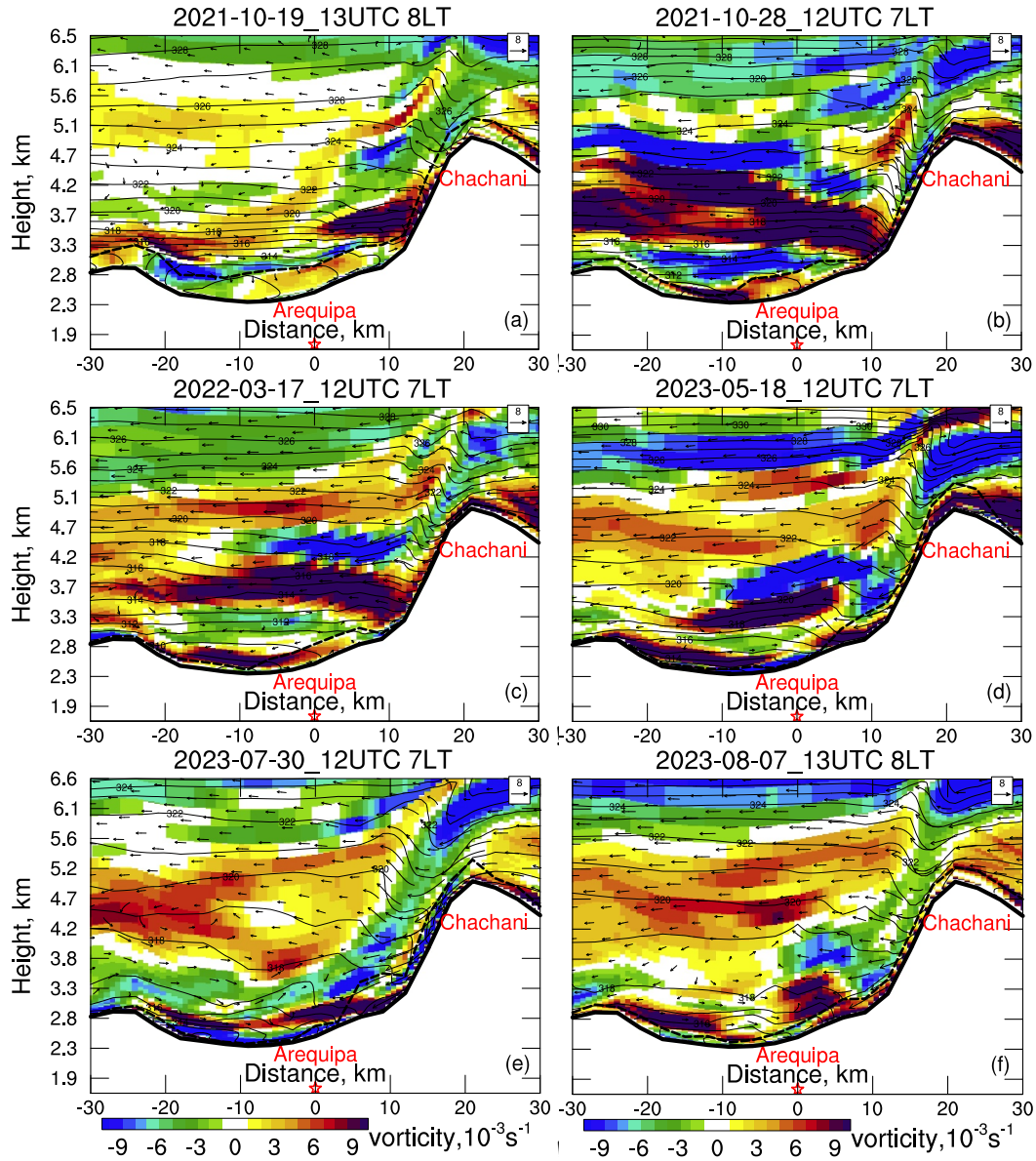

Figure 9. South-north cross-section of vorticity, winds, and potential temperature through Arequipa and Mountain Chachani during early morning on (a) October 19 and (b) 28, 2021; (c) 17 March 2022; and (d) May 18, (e) July 30, and (f) 7 August 2023. The boundary layer top is marked using the black dash lines.

morning plumes during all the other cases spread above the stable boundary layer, not penetrating through the top of the boundary layer (Figure 7).

Nighttime downward transport of SO_2 plumes facilitated by the gravity waves is further confirmed by a WRF-Chem sensitivity simulation removing Mountain Chachani for the case of 30 July 2023. This case has the widest early morning spread of SO_2 plumes into the Arequipa valley. With Chachani removed, the nighttime downslope transport of the SO_2 plume is less prominent and the SO_2 plume in the Arequipa valley is less widespread in the morning of 30 July 2023 (Figure 10).

Such mountain-facilitated downward transport of SO_2 plumes by the downslope winds linked to mountain gravity waves and by reversed local circulations occur mostly during late night and early mornings. In addition to the case of July 30 seen in Figure 10, time evolution of the waves and local circulations for the case of 28 October 2021 is illustrated in Figure 11 more clearly by focusing on/shading potential temperature rather than SO_2. At 03 LST

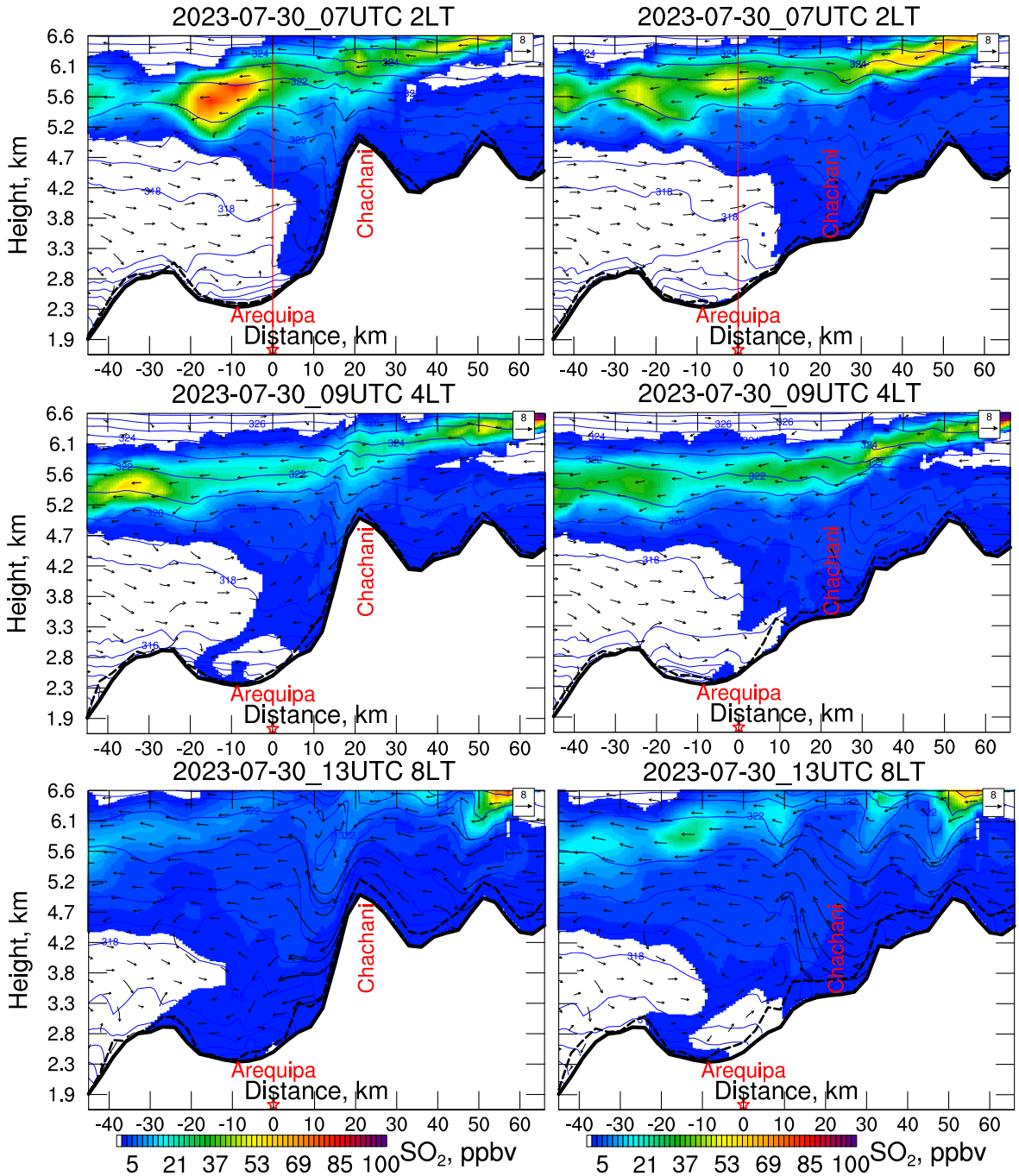

Figure 10. South-north cross-section of SO_2 (shaded), winds (vectors), and potential temperature (contours) through Arequipa and Mountain Chachani at (top–bottom) 2, 4, and 8 LT on 30 July 2023 (left) with Chachani and (right) without Chachani. The boundary layer top is marked using the black dash lines. Red vertical lines over Arequipa are draw in the top panel to measure the distance of the SO_2 plume from Arequipa.

(Figure 11a), a near-surface stable layer is established on the mountain top north of the Chachani peak and within the valley while the gravity wave motion is still weaker. By 04 LST (Figure 11b), the wave amplitudes have increased significantly, with the downslope flow off the mountain peak on the lee side fully developed. The rapid amplification of the waves with rapid downslope descent is likely due to the occurrence of overturning at ~ 6 km level, as evidenced by the nearly vertical isentropes there. At 04 LST, there is a thin stable boundary layer above the terrain profile, due to nighttime cooling. This process would create a thin layer of drainage flow on the lee slope, which will enhance the downslope flow, bringing some higher-level air with SO_2 to lower levels, and the

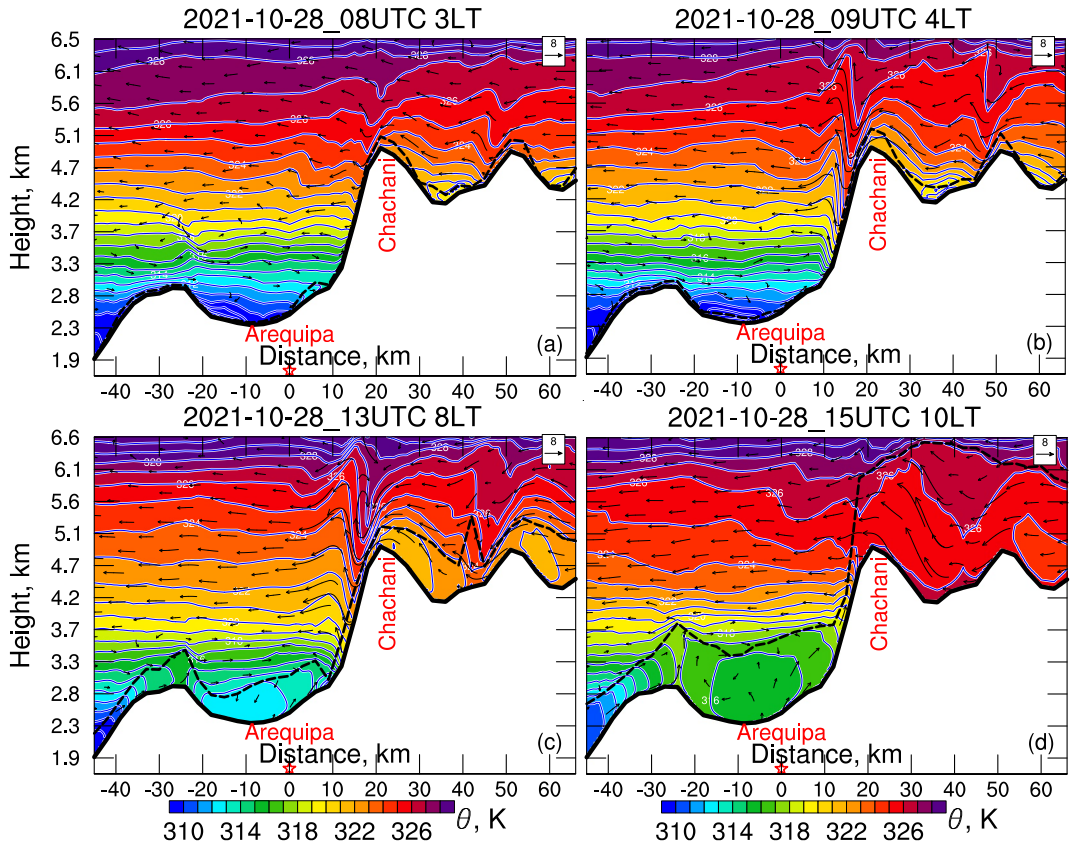

Figure 11. Time evolution of the south-north cross-section of potential temperature (shaded) and winds (vectors) through Arequipa and Mountain Chachani at (a) 3, (b) 4, (c) 8, and (d) 10 LT on 28 October 2021. The boundary layer top is marked using the black dash lines.

adiabatic cooling would allow the air parcels to cross the isentropes. By 08 LST (Figure 11c), the downslope flow has significantly weakened, likely related to the erosion of near-surface stable layer before the mountain peak due to near morning warming. The surface temperature in the valley has also increased by several degrees, the boundary layer depth has increased significantly, and the boundary layer becomes mostly neutrally stable. By this time, the aloft SO_2 plume has propagated halfway the lee slope (Figure 7). By 10 LST (Figure 11d), the boundary layer warming continues, and the temperature is increased by 3–4° upstream of the mountain top and in the valley. The weak stratification upstream of the mountain peak prevents the formation of strong mountain gravity waves on the lee side so that the downslope flow there has essentially disappeared and there is an indication of weak upslope flows on the lower to the middle lee slope by the upward bending/bulging of isentropes, due to upward advection of lower potential temperature air. Within the valley, the well-mixed boundary layer is more than 1 km deep, and such daytime mixing can easily mix SO_2-rich air above down to the surface as discussed next.

Even though the gravity waves and the associated downslope winds subside in early morning, some of the SO_2 plumes spreading above the stable boundary layer may be further transported to near the surface during the day when the convective boundary layer keeps growing, for example, 17 March 2022, and 7 August 2023 (two cases when daytime downward transport of SO_2 through vertical mixing is mostly clearly identified) as illustrated in Figure 12. At 9 LT, the SO_2 plume stays above the boundary layer on 17 March 2022, while the SO_2 plume starts to be transported/mixed to the Chili River valley to the south of Arequipa on 7 August 2023. When the convective boundary layer grows high enough (>1 km above the ground at 10 LT for the two cases) due to turbulent eddy mixing (Stull, 1988) to approach the SO_2 plumes above, the SO_2-rich air is entrained into the convective boundary layer and mixed down to the surface (Figure 12), affecting the air quality in the Arequipa city. As a result, the near-surface air quality is directly affected by the main volcano SO_2 plumes higher up in the free troposphere by 11 LT, and such a mixing process continues into afternoon, bringing down more SO_2 to the surface (Figure 12). The enhancement to near-surface air pollution through boundary layer top entrainment and downward mixing of

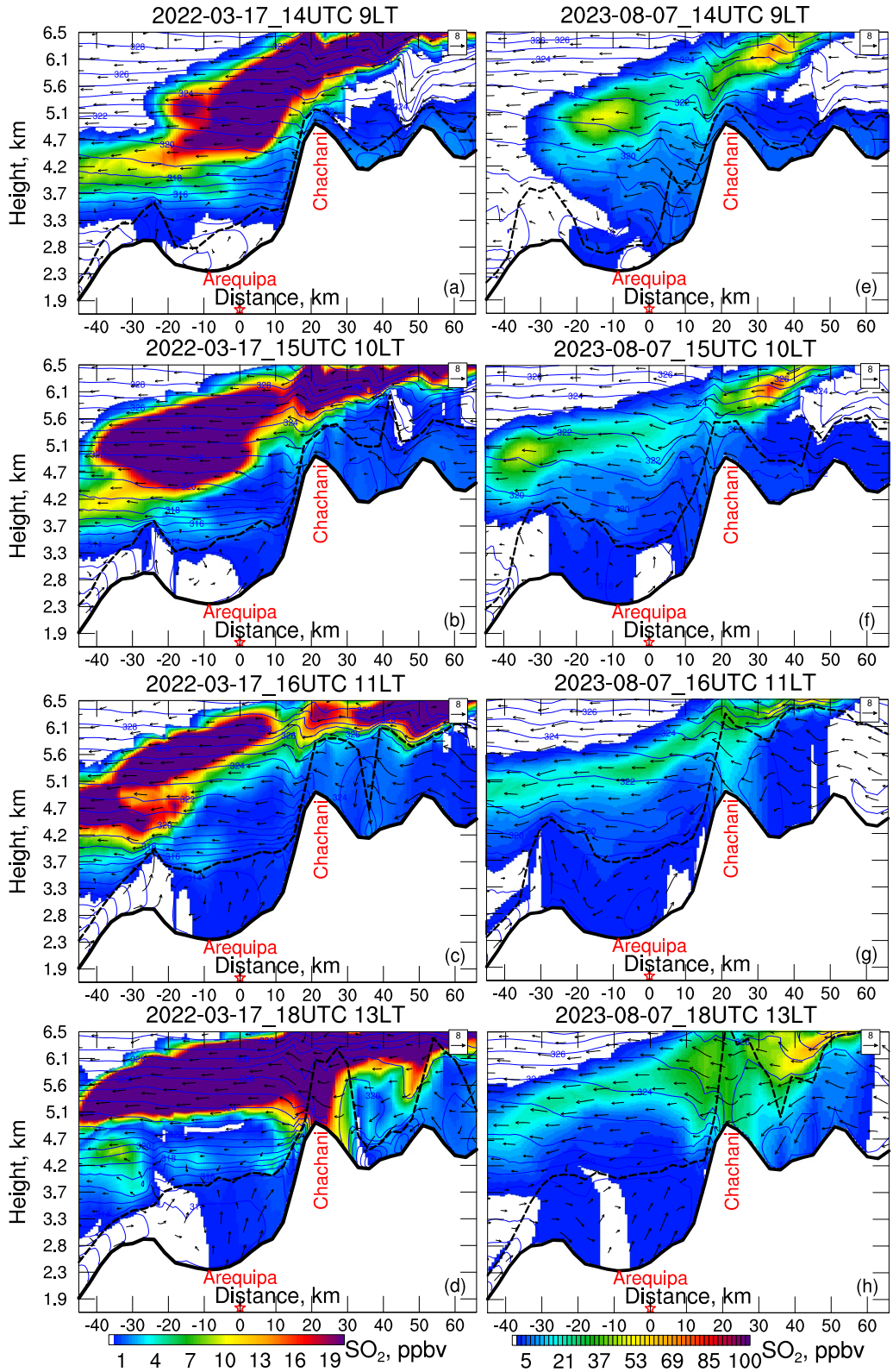

Figure 12. Downward transport of SO_2 to Arequipa when the convective boundary layer grows at (a and e) 9, (b and f) 10, and (c and g) 11 LT, (d and h) 13 LT on (left) 17 March 2022 and (right) 7 August 2023. The boundary layer top is marked using the black dash lines.

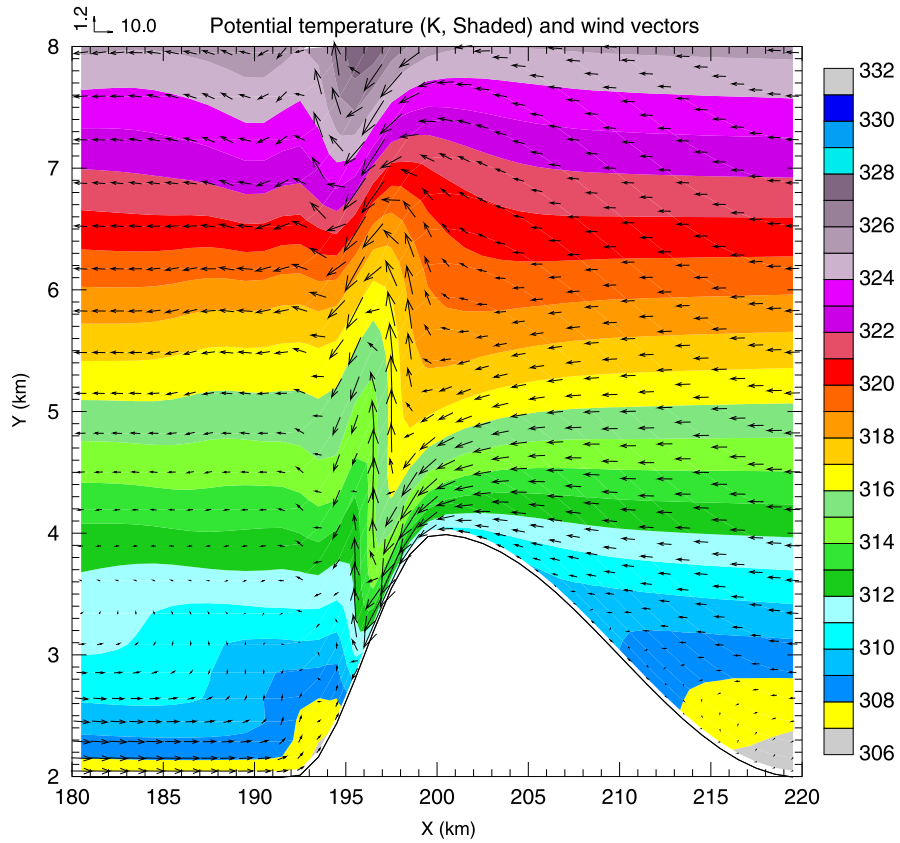

Figure 13. South-north vertical cross-section of potential temperature and wind fields through the mountain peak simulated by ARPS after 4 hr of integration.

polluted air higher up during morning hours when the boundary layer deepens has been documented in many earlier studies (Aneja et al., 2000; Hu et al., 2013, 2018; Morris et al., 2010; Neu et al., 1994; Tong et al., 2011; Yorks et al., 2009; Zhang et al., 1998; Zhang & Rao, 1999). Such a mechanism was illustrated in a single-column model study by Hu et al. (2013).

Another feature worth noting is the general downward slope of the main midtroposphere SO_2 plumes on the downwind side of the Chachani Mountain (Figure 12). The weak descent of the main SO_2 plumes appears to have played some role. More important is likely the mountain-valley circulation that develops during the day that is counterclockwise in the plots—the thermally driven upslope circulation toward the Chachani Mountain top seen in Figure 12 would induce downward motion at the middle levels above the valley. This downward motion will also help lower the SO_2 plumes, for them to be more easily reached and entrained into the boundary layer during daytime. These are named as the mountain venting processes (De Wekker et al., 2004; Steyn et al., 2013).

3.3. Air Flows in an Idealized Simulation Considering Mountain Dynamic Effect Only

The WRF-Chem simulations analyzed above use real complex terrain and involve both dynamic and thermal forcing of the mountain surface. To illustrate the effect of pure dynamic forcing by the mountain peak like that of Mount Chachani on a stable flow over the mountain, we perform an idealized simulation using the ARPS model (Xue et al., 2000, 2001, 2003) that had been shown to work well for this type of problem (Doyle et al., 2000). The 2-km asymmetric bell-shaped mountain sits on a plateau of 2 km above sea level (see Figure 13), mimicking Mount Chachani rising above the lower-lying Arequipa valley (Figure 12). Figure 13 shows the simulated wind vectors in the vertical cross-section trough the mountain peak, and the potential temperature contours that approximately represent the flow streamlines. The simulated flow has roughly reached a steady state by this time.

Flows over the idealized mountain are dominated by the large-amplitude mountain wave feature above the lee slope in the presence of a stable stratification. The flow over the upper part of the slope features flow overturning

with nearly vertical isentropes, as a response of stable flow passing over a tall mountain (Figure 13). Such flow structures are similar to that over Mount Chachani during nighttime and early morning. The 312-K isentrope descends by about 1 km over the lee slope in the simulation (Figure 13), similar to the real case simulations (Figure 11b) discussed earlier. Thus, this idealized simulation further confirms that the dynamic forcing of Mount Chachani plays an important role to induce the downslope flow on the upper part of the lee slope as part of the high-amplitude mountain gravity wave response. The downslope winds bring the SO_2 plumes from the mid-troposphere to the lower levels, where the SO_2 plumes can be further transported by a thin-layer nighttime drainage flow in the real case and mixed downward by daytime boundary mixing, leading to SO_2 pollution within the Arequipa valley on some days.

4. Conclusions and Discussion

TROPOMI data suggest volcano Sabancaya (elevation 5,960 m, ~80 km north to Arequipa) emits significant amount of SO_2 with ~4,000 ton of SO_2 drifting in the air over the Arequipa region on a daily base. This study aims to examine whether such SO_2 plumes can be brought down to the lower-lying Arequipa city, thus exacerbating ambient air quality in this mountainous region. For the first time, we use WRF-Chem simulations to reveal that in the presence of favorable meteorological conditions, the plumes from volcano Sabancaya can be brought to Arequipa through a series of transport and dispersion processes. (a) In presence of northerly/northwesterly winds the free troposphere plume from Sabancaya is intercepted by Mount Chachani (summit elevation of 6,057 m, ~20 km north to Arequipa) and is widely spread over elevated mountainous regions during daytime through convective boundary layer growth and the mountain venting process related to upvalley/upslope flows and the corresponding compensation circulations. These SO_2-rich mountainous air mass is further transported downward to Arequipa by downslope winds behind the gravity wave over the upper slope induced by the mountain's dynamic effect during nighttime. The downslope motion is likely aided by nighttime drainage flows in a thin layer near the surface over the lower part of the slope due to nighttime cooling. Often the plume is downward transported to above the boundary layer over Arequipa until the strong stratification of stable boundary layer prevents the downward transport. (b) On the following day, convective boundary layer growth and mountain venting process further transport the plume above the boundary layer to near the surface through entrainment and vertical mixing processes, thus exacerbating ambient air pollution over Arequipa. Idealized flow simulation over a bell-shaped mountain using the ARPS model excluding the mountain's thermal effect but considering dynamic effect only further confirms that the nighttime wave motion is indeed induced by mountain's dynamic effect.

The air pollution formation mechanism revealed in this study has implications for air quality management and public health in Arequipa. Convective boundary layer growth in the morning plays an important role to transport the SO_2 plumes at the boundary layer top downward to exacerbate surface air pollution of SO_2 and secondary aerosols. Such a boundary layer process was also reported to exacerbate surface O_3 pollution rapidly in the morning in many regions around the world (Aneja et al., 2000; Athanassiadis et al., 2002; Hu et al., 2013; Morris et al., 2010; Zhang & Rao, 1999). Thus, air quality management during the early morning boundary layer growth period is critical to mitigate these pollutants to protect public health. Mountain effects also play important roles for the air pollution in the Arequipa region; thus, the discovered air pollution mechanism may also help understand the air pollution in other mountainous regions (Hu et al., 2014; Li, Miao, et al., 2021; Steyn et al., 2013).

Explicit comparisons with the air pollution impact of other volcanoes are also worthwhile for future studies. Because most volcano eruption plumes exist in the free troposphere and stratosphere, previous studies mostly focused on climate impact of volcano plumes, with limited research on impact of volcano plumes on air quality near the surface discussing a few low elevation volcanoes. Volcano plumes injected to the upper troposphere (>5 km above sea level) were presumed unlikely to impact surface air quality (Thomas et al., 2017). This modeling study discovers a mechanism of how the daily volcano Sabancaya's degassing plumes between ~6 and 10 km above sea level exacerbates air pollution over Arequipa, a mountainous region, focusing on SO_2 as a first attempt. A mountain's dynamic effect is shown to play an important role in the downward transport of the plumes. Further research regarding mountain effects including both dynamic and thermal effects on other environments such as meteorology and local climate in addition to air quality is needed in this mountainous region. More quantitative studies estimating contribution of volcano plumes to ambient aerosol pollution are warranted using model simulations including aerosol processes and more accurate volcano emissions in terms of total amount and vertical distribution (e.g., Tang et al., 2020). SO_2 partially contributes to the aerosol pollution through gas-phase oxidization and the subsequent gas-particle mass transfer process as well as aqueous-phase oxidization (Graf

et al., 1997; Hu et al., 2008; von Glasow et al., 2009). Future research could examine the impact of volcano emissions on both gas- and aerosol-phase pollutants through aerosol-including simulations.

Data Availability Statement

The Sentinel-5P TROPOMI Sulphur Dioxide data (Fioletov et al., 2020) are available at https://disc.gsfc.nasa.gov/datasets/S5P_L2__SO2____HiR_2/summary?keywords=S5P%20SO2. The sounding data are provided by Servicio Nacional de Meteorología e Hidrología del Perú (SENAMHI), Arequipa, Perú (Jara, 2024). Model data produced from this study (Hu, 2025) have been archived at CAPS website https://caps.ou.edu/micronet/Peru.html and the Luster NSF projects data server at the San Diego Supercomputer Center, /expanse/luster/projects/uok114/xhu2.

Acknowledgments
This work was primarily supported by Grant 20163646499 from the Universidad Nacional de San Agustín de Arequipa (UNSA) of Peru through the IREES/LASI Global Change and Human Health Institute. The first author is partially supported by the DOE ASR project (DE-SC0021159). Ming Xue was also supported by NSF Grant AGS-1917701. The WRF simulations were performed on the supercomputer Stampede 3 at the Texas Advanced Computing Center (TACC) through allocation TG-ATM160014 from the Advanced Cyberinfrastructure Coordination Ecosystem: Services & Support (ACCESS) program, which is supported by National Science Foundation Grants #2138259, #2138286, #2138307, #2137603, and #2138296. Postprocessing of TROPOMI Sulphur Dioxide data for this work was performed on the supercomputer Expanse at the San Diego Supercomputer Center (SDSC).

References

An, J. L., Ueda, H., Matsuda, K., Hasome, H., & Iwata, M. (2003). Simulated impacts of SO_2 emissions from the Miyake volcano on concentration and deposition of sulfur oxides in September and October of 2000. *Atmospheric Environment*, *37*(22), 3039–3046. https://doi.org/10.1016/s1352-2310(03)00327-3

Aneja, V. P., Mathur, R., Arya, S. P., Li, Y., Murray, G. C., & Manuszak, T. L. (2000). Coupling the vertical distribution of ozone in the atmospheric boundary layer. *Environmental Science & Technology*, *34*(11), 2324–2329. https://doi.org/10.1021/es990997+

Athanassiadis, G. A., Rao, S. T., Ku, J.-Y., & Clark, R. D. (2002). Boundary layer evolution and its influence on ground-level ozone concentrations. *Environmental Fluid Mechanics*, *2*(4), 339–357. https://doi.org/10.1023/A:1020456018087

Baines, P. G. (1998). *Topographic effects in stratified flows*. Cambridge University Press.

Bao, X., Zhang, F., & Sun, J. (2011). Diurnal variations of warm-season precipitation East of the Tibetan Plateau over China. *Monthly Weather Review*, *139*(9), 2790–2810. https://doi.org/10.1175/MWR-D-11-00006.1

Bluestein, H. B. (1992). *Synoptic-dynamic meteorology in midlatitudes: Observations and theory of weather systems*. Oxford University Press.

Bonin, T. A., Klein, P. M., & Chilson, P. B. (2020). Contrasting characteristics and evolution of southerly low-level jets during different boundary-layer regimes. *Boundary-Layer Meteorology*, *174*(2), 179–202. https://doi.org/10.1007/s10546-019-00481-0

Braun, S. A., Rotunno, R., & Klemp, J. B. (1999). Effects of coastal orography on landfalling cold fronts. Part I: Dry, inviscid dynamics. *Journal of the Atmospheric Sciences*, *56*(4), 517–533. https://doi.org/10.1175/1520-0469(1999)056<0517:Eocool>2.0.Co;2

Burton, M. R., Sawyer, G. M., & Granieri, D. (2013). Deep carbon emissions from volcanoes. *Reviews in Mineralogy and Geochemistry*, *75*(1), 323–354. https://doi.org/10.2138/rmg.2013.75.11

Carbo-Bustinza, N., Belmonte, M., Jimenez, V., Montalban, P., Rivera, M., Martínez, F. G., et al. (2022). A machine learning approach to analyse ozone concentration in metropolitan area of Lima, Peru. *Scientific Reports*, *12*(1), 22084. https://doi.org/10.1038/s41598-022-26575-3

Carn, S. A., Fioletov, V. E., McLinden, C. A., Li, C., & Krotkov, N. A. (2017). A decade of global volcanic SO_2 emissions measured from space. *Scientific Reports*, *7*(1), 44095. https://doi.org/10.1038/srep44095

Cazorla, M., Gallardo, L., & Jimenez, R. (2022). The complex Andes region needs improved efforts to face climate extremes. *Elementa: Science of the Anthropocene*, *10*(1). https://doi.org/10.1525/elementa.2022.00092

Chow, F. K., De Wekker, S. F. J., & Snyder, B. J. (2012). *Mountain weather research and forecasting: Recent progress and current challenges*. Springer Netherlands.

Colla, N. S. L., Botté, S. E., & Marcovecchio, J. E. (2021). Atmospheric particulate pollution in South American megacities. *Environmental Reviews*, *29*(3), 415–429. https://doi.org/10.1139/er-2020-0105

Colle, B. A., Smull, B. F., & Yang, M. J. (2002). Numerical simulations of a landfalling cold front observed during COAST: Rapid evolution and responsible mechanisms. *Monthly Weather Review*, *130*(8), 1945–1966. https://doi.org/10.1175/1520-0493(2002)130<1945:Nsoalc>2.0.Co;2

Crawford, B., Hagan, D. H., Grossman, I., Cole, E., Holland, L., Heald, C. L., & Kroll, J. H. (2021). Mapping pollution exposure and chemistry during an extreme air quality event (the 2018 K=ilauea eruption) using a low-cost sensor network. *Proceedings of the National Academy of Sciences of the United States of America*, *118*(27). https://doi.org/10.1073/pnas.2025540118

de Moura, F. R., & da Silva Júnior, F. M. R. (2023). 2030 Agenda: Discussion on Brazilian priorities facing air pollution and climate change challenges. *Environmental Science and Pollution Research*, *30*(3), 8376–8390. https://doi.org/10.1007/s11356-022-24601-5

De Wekker, S. F. J., Steyn, D. G., & Nyeki, S. (2004). A comparison of aerosol-layer and convective boundary-layer structure over a mountain range during Staaarte '97. *Boundary-Layer Meteorology*, *113*(2), 249–271. https://doi.org/10.1023/B:BOUN.0000039371.41823.37

Doyle, J. D. (1997). The influence of mesoscale orography on a coastal jet and rainband. *Monthly Weather Review*, *125*(7), 1465–1488. https://doi.org/10.1175/1520-0493(1997)125<1465:Tiomoo>2.0.Co;2

Doyle, J. D., Durran, D. R., Chen, C., Colle, B. A., Georgelin, M., Grubisic, V., et al. (2000). An intercomparison of model-predicted wave breaking for the 11 January 1972 boulder windstorm. *Monthly Weather Review*, *128*(3), 901–914. https://doi.org/10.1175/1520-0493(2000)128<0901:AIOMPW>2.0.CO;2

Durran, D. R. (1986). Another look at downslope windstorms. Part I: The development of analogs to supercritical flow in an infinitely deep, continuously stratified fluid. *Journal of the Atmospheric Sciences*, *43*(21), 2527–2543. https://doi.org/10.1175/1520-0469(1986)043<2527:ALADWP>2.0.CO;2

Dutton, E. G., & Christy, J. R. (1992). Solar radiative forcing at selected locations and evidence for global lower tropospheric cooling following the eruptions of El Chichón and Pinatubo. *Geophysical Research Letters*, *19*(23), 2313–2316. https://doi.org/10.1029/92GL02495

Emery, B. R., Montague, D. C., Field, R. A., & Parish, T. R. (2015). Barrier wind formation in the upper green river basin of Sublette county, Wyoming, and its relationship to elevated ozone distributions in winter. *Journal of Applied Meteorology and Climatology*, *54*(12), 2427–2442. https://doi.org/10.1175/jamc-d-15-0103.1

Epifanio, C. C., & Qian, T. (2008). Wave–turbulence interactions in a breaking mountain wave. *Journal of the Atmospheric Sciences*, *65*(10), 3139–3158. https://doi.org/10.1175/2008JAS2517.1

Epifanio, C. C., & Rotunno, R. (2005). The dynamics of orographic wake formation in flows with upstream blocking. *Journal of the Atmospheric Sciences*, *62*(9), 3127–3150. https://doi.org/10.1175/JAS3523.1

Fast, J. D., Gustafson, W. I., Jr., Easter, R. C., Zaveri, R. A., Barnard, J. C., Chapman, E. G., et al. (2006). Evolution of ozone, particulates, and aerosol direct radiative forcing in the vicinity of Houston using a fully coupled meteorology-chemistry-aerosol model. *Journal of Geophysical Research*, *111*(D21). https://doi.org/10.1029/2005jd006721

Feron, S., Cordero, R. R., Damiani, A., Oyola, P., Ansari, T., Pedemonte, J. C., et al. (2023). Compound climate-pollution extremes in Santiago de Chile. *Scientific Reports*, *13*(1), 6726. https://doi.org/10.1038/s41598-023-33890-w

Filonchyk, M., Peterson, M. P., Gusev, A., Hu, F., Yan, H., & Zhou, L. (2022). Measuring air pollution from the 2021 Canary Islands volcanic eruption. *Science of the Total Environment*, *849*, 157827. https://doi.org/10.1016/j.scitotenv.2022.157827

Fioletov, V., McLinden, C. A., Griffin, D., Theys, N., Loyola, D. G., Hedelt, P., et al. (2020). Anthropogenic and volcanic point source SO_2 emissions derived from TROPOMI on board Sentinel-5 Precursor: First results [Dataset]. *Atmospheric Chemistry and Physics*, *20*(9), 5591–5607. https://doi.org/10.5194/acp-20-5591-2020

Fioletov, V. E., McLinden, C. A., Krotkov, N., Li, C., Joiner, J., Theys, N., et al. (2016). A global catalogue of large SO_2 sources and emissions derived from the Ozone Monitoring Instrument. *Atmospheric Chemistry and Physics*, *16*(18), 11497–11519. https://doi.org/10.5194/acp-16-11497-2016

Free, M., & Robock, A. (1999). Global warming in the context of the little Ice Age. *Journal of Geophysical Research*, *104*(D16), 19057–19070. https://doi.org/10.1029/1999JD900233

Gao, C., Ludlow, F., Matthews, J. A., Stine, A. R., Robock, A., Pan, Y., et al. (2021). Volcanic climate impacts can act as ultimate and proximate causes of Chinese dynastic collapse. *Communications Earth & Environment*, *2*(1), 234. https://doi.org/10.1038/s43247-021-00284-7

Gettelman, A., Mills, M. J., Kinnison, D. E., Garcia, R. R., Smith, A. K., Marsh, D. R., et al. (2019). The Whole Atmosphere Community Climate Model Version 6 (WACCM6). *Journal of Geophysical Research: Atmospheres*, *124*(23), 12380–12403. https://doi.org/10.1029/2019JD030943

Global Volcanism Program. (2022). Report on Sabancaya (Peru). In K. L. Bennis & B. Andrews (Eds.), *Bulletin of the Global Volcanism Network* (Vol. 47, p. 5). Smithsonian Institution. https://doi.org/10.5479/si.GVP.BGVN202205-354006

Gómez Peláez, L. M., Santos, J. M., de Almeida Albuquerque, T. T., Reis, N. C., Andreão, W. L., & de Fátima Andrade, M. (2020). Air quality status and trends over large cities in South America. *Environmental Science & Policy*, *114*, 422–435. https://doi.org/10.1016/j.envsci.2020.09.009

Graf, H.-F., Feichter, J., & Langmann, B. (1997). Volcanic sulfur emissions: Estimates of source strength and its contribution to the global sulfate distribution. *Journal of Geophysical Research*, *102*(D9), 10727–10738. https://doi.org/10.1029/96JD03265

Gregori, G. P. (1995). Remote sensing of volcanoes and their role in the global climate change. *Advances in Space Research*, *15*(11), 17–26. https://doi.org/10.1016/0273-1177(95)00071-L

Grell, G. A., Peckham, S. E., Schmitz, R., McKeen, S. A., Frost, G., Skamarock, W. C., & Eder, B. (2005). Fully coupled "online" chemistry within the WRF model. *Atmospheric Environment*, *39*(37), 6957–6975. https://doi.org/10.1016/j.atmosenv.2005.04.027

Harden, B. E., Renfrew, I. A., & Petersen, G. N. (2011). A climatology of wintertime barrier winds off southeast Greenland. *Journal of Climate*, *24*(17), 4701–4717. https://doi.org/10.1175/2011jcli4113.1

He, H., & Zhang, F. (2010). Diurnal variations of warm-season precipitation over northern China. *Monthly Weather Review*, *138*(4), 1017–1025. https://doi.org/10.1175/2010MWR3356.1

Hegerl, G. C., Crowley, T. J., Baum, S. K., Kim, K.-Y., & Hyde, W. T. (2003). Detection of volcanic, solar and greenhouse gas signals in paleo-reconstructions of Northern Hemispheric temperature. *Geophysical Research Letters*, *30*(5). https://doi.org/10.1029/2002GL016635

Hidayati, D., Ismail, B. S., Shuhaimi-Othman, M., & Sulaiman, N. (2018). chemical composition of a mud volcano LUSI and the health risk involved based on the air quality index that occurred as a result of disastrous gas exploration drilling activities in Sidoarjo, Indonesia. *Sains Malaysiana*, *47*(8), 1665–1674. https://doi.org/10.17576/jsm-2018-4708-05

Holland, L., Businger, S., Elias, T., & Cherubini, T. (2020). Two ensemble approaches for forecasting sulfur dioxide concentrations from Kilauea Volcano. *Weather and Forecasting*, *35*(5), 1923–1937. https://doi.org/10.1175/waf-d-19-0189.1

Holt, T. R. (1996). Mesoscale forcing of a boundary layer jet along the California coast. *Journal of Geophysical Research*, *101*(D2), 4235–4254. https://doi.org/10.1029/95jd03231

Hong, S. Y., Noh, Y., & Dudhia, J. (2006). A new vertical diffusion package with an explicit treatment of entrainment processes. *Monthly Weather Review*, *134*(9), 2318–2341. https://doi.org/10.1175/Mwr3199.1

Hu, J., Li, Y. C., Zhao, T. L., Liu, J., Hu, X.-M., Liu, D. Y., et al. (2018). An important mechanism of regional O-3 transport for summer smog over the Yangtze River Delta in eastern China. *Atmospheric Chemistry and Physics*, *18*(22), 16239–16251. https://doi.org/10.5194/acp-18-16239-2018

Hu, X.-M. (2025). Outputs of WRF-Chem simulations over Peru [Dataset]. *CAPS*. Retrieved from https://caps.ou.edu/micronet/Peru.html

Hu, X.-M., Huang, Y., Xue, M., Martin, E., Hong, Y., Chen, M., et al. (2023). Effects of lower troposphere vertical mixing on simulated clouds and precipitation over the Amazon during the wet season. *Journal of Geophysical Research: Atmospheres*, *128*(12), e2023JD038553. https://doi.org/10.1029/2023JD038553

Hu, X.-M., Klein, P. M., Xue, M., Zhang, F., Doughty, D. C., Forkel, R., et al. (2013). Impact of the vertical mixing induced by low-level jets on boundary layer ozone concentration. *Atmospheric Environment*, *70*, 123–130. https://doi.org/10.1016/j.atmosenv.2012.12.046

Hu, X.-M., Li, X. L., Xue, M., Wu, D., & Fuentes, J. D. (2016). The formation of barrier winds east of the Loess Plateau and their effects on dispersion conditions in the North China Plains. *Boundary-Layer Meteorology*, *161*(1), 145–163. https://doi.org/10.1007/s10546-016-0159-4

Hu, X.-M., Ma, Z. Q., Lin, W. L., Zhang, H. L., Hu, J. L., Wang, Y., et al. (2014). Impact of the Loess Plateau on the atmospheric boundary layer structure and air quality in the North China Plain: A case study. *Science of the Total Environment*, *499*, 228–237. https://doi.org/10.1016/j.scitotenv.2014.08.053

Hu, X.-M., Zhang, Y., Jacobson, M. Z., & Chan, C. K. (2008). Coupling and evaluating gas/particle mass transfer treatments for aerosol simulation and forecast. *Journal of Geophysical Research*, *113*(D11), D11208. https://doi.org/10.1029/2007jd009588

Huamán De La Cruz, A., Bendezu Roca, Y., Suarez-Salas, L., Pomalaya, J., Alvarez Tolentino, D., & Gioda, A. (2019). Chemical characterization of $PM_{2.5}$ at rural and urban sites around the metropolitan area of Huancayo (Central Andes of Peru). *Atmosphere*, *10*(1), 21. https://doi.org/10.3390/atmos10010021

Huang, Y., Xue, M., Hu, X.-M., Martin, E., Novoa, H. M., McPherson, R. A., et al. (2024). Characteristics of precipitation and mesoscale convective systems over the Peruvian Central Andes in multi 5-year convection-permitting simulations. *Journal of Geophysical Research: Atmospheres*, *129*(17), e2023JD040394. https://doi.org/10.1029/2023JD040394

Huang, Y., Xue, M., Hu, X.-M., Martin, E., Novoa, H. M., McPherson, R. A., et al. (2023). Convection-permitting simulations of precipitation over the Peruvian Central Andes: Strong sensitivity to planetary boundary layer parameterization. *Journal of Hydrometeorology*, *24*(11), 1969–1990. https://doi.org/10.1175/JHM-D-22-0173.1

Iacono, M. J., Delamere, J. S., Mlawer, E. J., Shephard, M. W., Clough, S. A., & Collins, W. D. (2008). Radiative forcing by long-lived greenhouse gases: Calculations with the AER radiative transfer models. *Journal of Geophysical Research*, *113*(D13). https://doi.org/10.1029/2008JD009944

Jackson, P. L., Mayr, G., & Vosper, S. (2013). Dynamically-driven winds. In F. K. Chow, S. F. J. De Wekker, & B. J. Snyder (Eds.), *Mountain Weather Research and Forecasting: Recent Progress and Current Challenges* (pp. 121–218). Springer.

Jara, J. L. T. (2024). Sounding data from Arequipa, Peru [Dataset]. *CAPS*. Retrieved from https://caps.ou.edu/micronet/Peru/Simulations/4.5.2/sounding_arequipaoct2023-20231020T152713Z-001.zip

Jiménez, P. A., Dudhia, J., González-Rouco, J. F., Navarro, J., Montávez, J. P., & García-Bustamante, E. (2012). A revised scheme for the WRF surface layer formulation. *Monthly Weather Review*, *140*(3), 898–918. https://doi.org/10.1175/mwr-d-11-00056.1

Jury, M. R., & Gaviria Pabón, A. R. (2021). Dispersion of smoke plumes over South America. *Earth Interactions*, *25*(1), 1–14. https://doi.org/10.1175/EI-D-20-0004.1

Kirchner, I., & Graf, H.-F. (1995). Volcanos and El Niño: Signal separation in Northern Hemisphere winter. *Climate Dynamics*, *11*(6), 341–358. https://doi.org/10.1007/BF00215736

Koukouli, M. E., Michailidis, K., Hedelt, P., Taylor, I. A., Inness, A., Clarisse, L., et al. (2022). Volcanic SO_2 layer height by TROPOMI/S5P: Evaluation against IASI/MetOp and CALIOP/CALIPSO observations. *Atmospheric Chemistry and Physics*, *22*(8), 5665–5683. https://doi.org/10.5194/acp-22-5665-2022

Larrea Valdivia, A. E., Reyes Larico, J. A., Salcedo Peña, J., & Wannaz, E. D. (2020). Health risk assessment of polycyclic aromatic hydrocarbons (PAHs) adsorbed in $PM_{2.5}$ and PM_{10} in a region of Arequipa, Peru. *Environmental Science and Pollution Research*, *27*(3), 3065–3075. https://doi.org/10.1007/s11356-019-07185-5

Li, J., & Chen, Y. L. (1998). Barrier jets during TAMEX. *Monthly Weather Review*, *126*(4), 959–971. https://doi.org/10.1175/1520-0493(1998)126<0959:Bjdt>2.0.Co;2

Li, J., Michalski, G., Olson, E. J., Welp, L. R., Larrea Valdivia, A. E., Larico, J. R., et al. (2021). Geochemical characterization and heavy metal sources in PM_{10} in Arequipa, Peru. *Atmosphere*, *12*(5), 641. https://doi.org/10.3390/atmos12050641

Li, X., Miao, Y., Ma, Y., Wang, Y., & Zhang, Y. (2021). Impacts of synoptic forcing and topography on aerosol pollution during winter in Shenyang, Northeast China. *Atmospheric Research*, *262*, 105764. https://doi.org/10.1016/j.atmosres.2021.105764

Li, X., Xia, X., Wang, L., Cai, R., Zhao, L., Feng, Z., et al. (2015). The role of foehn in the formation of heavy air pollution events in Urumqi, China. *Journal of Geophysical Research: Atmospheres*, *120*(11), 5371–5384. https://doi.org/10.1002/2014JD022778

Loescher, K. A., Young, G. S., Colle, B. A., & Winstead, N. S. (2006). Climatology of barrier jets along the Alaskan coast. Part 1: Spatial and temporal distributions. *Monthly Weather Review*, *134*(2), 437–453. https://doi.org/10.1175/Mwr3037.1

Lu, H., Xie, M., Liu, B., Liu, X., Feng, J., Yang, F., et al. (2022). Impact of atmospheric thermodynamic structures and aerosol radiation feedback on winter regional persistent heavy particulate pollution in the Sichuan-Chongqing region, China. *Science of the Total Environment*, *842*, 156575. https://doi.org/10.1016/j.scitotenv.2022.156575

Mann, M. E., Bradley, R. S., & Hughes, M. K. (1998). Global-scale temperature patterns and climate forcing over the past six centuries. *Nature*, *392*(6678), 779–787. https://doi.org/10.1038/33859

Markus, B., Valade, S., Wöllhaf, M., & Hellwich, O. (2023). Automatic retrieval of volcanic SO_2 emission source from TROPOMI products. *Frontiers in Earth Science*, *10*. https://doi.org/10.3389/feart.2022.1064171

Marshall, L. R., Maters, E. C., Schmidt, A., Timmreck, C., Robock, A., & Toohey, M. (2022). Volcanic effects on climate: Recent advances and future avenues. *Bulletin of Volcanology*, *84*(5), 54. https://doi.org/10.1007/s00445-022-01559-3

McCormick, M. P., Thomason, L. W., & Trepte, C. R. (1995). Atmospheric effects of the Mt Pinatubo eruption. *Nature*, *373*(6513), 399–404. https://doi.org/10.1038/373399a0

Michalski, G., Valdivia, A. E. L., Olson, E., Welp, L., Fang, H., Magara-Gomez, K., et al. (2022). Identifying NOx sources in Arequipa, Peru using nitrogen isotopes in particulate nitrate. *Frontiers in Environmental Science*, *10*, 916738. https://doi.org/10.3389/fenvs.2022.916738

Morris, G. A., Ford, B., Rappenglück, B., Thompson, A. M., Mefferd, A., Ngan, F., & Lefer, B. (2010). An evaluation of the interaction of morning residual layer and afternoon mixed layer ozone in Houston using ozonesonde data. *Atmospheric Environment*, *44*(33), 4024–4034. https://doi.org/10.1016/j.atmosenv.2009.06.057

Moussallam, Y., Tamburello, G., Peters, N., Apaza, F., Schipper, C. I., Curtis, A., et al. (2017). Volcanic gas emissions and degassing dynamics at Ubinas and Sabancaya volcanoes; implications for the volatile budget of the central volcanic zone. *Journal of Volcanology and Geothermal Research*, *343*, 181–191. https://doi.org/10.1016/j.jvolgeores.2017.06.027

National Centers for Environmental Prediction. (2015). NCEP GDAS/FNL 0.25 degree global tropospheric analyses and forecast grids. https://doi.org/10.5065/D65Q4T4Z

Nawaz, M. O., & Henze, D. K. (2020). Premature deaths in brazil associated with long-term exposure to $PM_{2.5}$ from Amazon fires between 2016 and 2019. *GeoHealth*, *4*(8), e2020GH000268. https://doi.org/10.1029/2020GH000268

Neu, U., Künzle, T., & Wanner, H. (1994). On the relation between ozone storage in the residual layer and daily variation in near-surface ozone concentration—A case study. *Boundary-Layer Meteorology*, *69*(3), 221–247. https://doi.org/10.1007/BF00708857

Nriagu, J. O. (1994). Mercury pollution from the past mining of gold and silver in the Americas. *Science of the Total Environment*, *149*(3), 167–181. https://doi.org/10.1016/0048-9697(94)90177-5

Olson, E., Michalski, G., Welp, L., Larrea Valdivia, A. E., Reyes Larico, J., Salcedo Peña, J., et al. (2021). Mineral dust and fossil fuel combustion dominate sources of aerosol sulfate in urban Peru identified by sulfur stable isotopes and water-soluble ions. *Atmospheric Environment*, *260*, 118482. https://doi.org/10.1016/j.atmosenv.2021.118482

Olson, J. B., & Colle, B. A. (2009). Three-dimensional idealized simulations of barrier jets along the southeast coast of Alaska. *Monthly Weather Review*, *137*(1), 391–413. https://doi.org/10.1175/2008mwr2480.1

Olson, J. B., Colle, B. A., Bond, N. A., & Winstead, N. (2007). A comparison of two coastal barrier jet events along the southeast Alaskan coast during the SARJET field experiment. *Monthly Weather Review*, *135*(8), 2973–2994. https://doi.org/10.1175/Mwr3448.1

Overland, J. E., & Bond, N. (1993). The influence of coastal orography—The Yakutat storm. *Monthly Weather Review*, *121*(5), 1388–1397. https://doi.org/10.1175/1520-0493(1993)121<1388:Tiocot>2.0.Co;2

Overland, J. E., & Bond, N. (1995). Observations and scale analysis of coastal wind jets. *Monthly Weather Review*, *123*(10), 2934–2941. https://doi.org/10.1175/1520-0493(1995)123<2934:Oasaoc>2.0.Co;2

Parish, T. R. (1983). The influence of the Antarctic Peninsula on the wind-field over the western weddell sea. *Journal of Geophysical Research-OceansAtmosphere*, *88*(Nc4), 2684–2692. https://doi.org/10.1029/Jc088ic04p02684

Pearce, J. L., Aguilar-Villalobos, M., Rathbun, S. L., & Naeher, L. P. (2009). Residential exposures to $PM_{2.5}$ and CO in Cusco, a high-altitude city in the Peruvian Andes: A pilot study. *Archives of Environmental & Occupational Health*, *64*(4), 278–282. https://doi.org/10.1080/19338240903338205

Peltier, W. R., & Clark, T. L. (1979). The evolution and stability of finite-amplitude mountain waves. Part II: Surface wave drag and severe downslope windstorms. *Journal of the Atmospheric Sciences*, *36*(8), 1498–1529. https://doi.org/10.1175/1520-0469(1979)036<1498:TEASOF>2.0.CO;2

Pu, B., & Dickinson, R. E. (2014). Diurnal spatial variability of great plains summer precipitation related to the dynamics of the low-level jet. *Journal of the Atmospheric Sciences*, *71*(5), 1807–1817. https://doi.org/10.1175/Jas-D-13-0243.1

Qian, T., Zhao, P., Zhang, F., & Bao, X. (2015). Rainy-season precipitation over the Sichuan basin and adjacent regions in southwestern China. *Monthly Weather Review*, *143*(1), 383–394. https://doi.org/10.1175/MWR-D-13-00158.1

Raible, C. C., Brönnimann, S., Auchmann, R., Brohan, P., Frölicher, T. L., Graf, H.-F., et al. (2016). Tambora 1815 as a test case for high impact volcanic eruptions: Earth system effects. *WIREs Climate Change*, *7*(4), 569–589. https://doi.org/10.1002/wcc.407

Richner, H., & Hächler, P. (2013). Understanding and forecasting Alpine Foehn. In F. K. Chow, S. F. J. De Wekker, & B. J. Snyder (Eds.), *Mountain Weather Research and Forecasting: Recent Progress and Current Challenges* (pp. 219–260). Springer.

Riojas-Rodríguez, H., Silva, A. S. d., Texcalac-Sangrador, J. L., & Moreno-Banda, G. L. (2016). Air pollution management and control in Latin America and the Caribbean: Implications for climate change. [Gestión y control de la contaminación atmosférica en América Latina y el Caribe: Implicaciones para el cambio climático]. *Revista Panamericana de Salud Públic*, *40*(3).

Saide, P. E., Carmichael, G. R., Spak, S. N., Gallardo, L., Osses, A. E., Mena-Carrasco, M. A., & Pagowski, M. (2011). Forecasting urban PM_{10} and $PM_{2.5}$ pollution episodes in very stable nocturnal conditions and complex terrain using WRF-Chem CO tracer model. *Atmospheric Environment*, *45*(16), 2769–2780. https://doi.org/10.1016/j.atmosenv.2011.02.001

Sandu, A., Daescu, D. N., & Carmichael, G. R. (2003). Direct and adjoint sensitivity analysis of chemical kinetic systems with KPP: Part I—Theory and software tools. *Atmospheric Environment*, *37*(36), 5083–5096. https://doi.org/10.1016/j.atmosenv.2003.08.019

Sandu, I., van Niekerk, A., Shepherd, T. G., Vosper, S. B., Zadra, A., Bacmeister, J., et al. (2019). Impacts of orography on large-scale atmospheric circulation. *Npj Climate and Atmospheric Science*, *2*(1), 10. https://doi.org/10.1038/s41612-019-0065-9

Schurer, A. P., Hegerl, G. C., Mann, M. E., Tett, S. F. B., & Phipps, S. J. (2013). Separating forced from Chaotic climate variability over the past millennium. *Journal of Climate*, *26*(18), 6954–6973. https://doi.org/10.1175/JCLI-D-12-00826.1

Schwerdtfeger, W. (1975). Effect of Antarctic Peninsula on temperature regime of Weddell Sea. *Monthly Weather Review*, *103*(1), 45–51. https://doi.org/10.1175/1520-0493(1975)103<0045:Teotap>2.0.Co;2

Shinohara, H. (2008). Excess degassing from volcanoes and its role on eruptive and intrusive activity. *Reviews of Geophysics*, *46*(4). https://doi.org/10.1029/2007RG000244

Shinohara, H. (2013). Volatile flux from subduction zone volcanoes: Insights from a detailed evaluation of the fluxes from volcanoes in Japan. *Journal of Volcanology and Geothermal Research*, *268*, 46–63. https://doi.org/10.1016/j.jvolgeores.2013.10.007

Silva, J. S., Rojas, J. P., Norabuena, M., & Seguel, R. J. (2018). Ozone and volatile organic compounds in the metropolitan area of Lima-Callao, Peru. *Air Quality, Atmosphere & Health*, *11*(8), 993–1008. https://doi.org/10.1007/s11869-018-0604-2

Skamarock, W. C., & Klemp, J. B. (2008). A time-split nonhydrostatic atmospheric model for weather research and forecasting applications. *Journal of Computational Physics*, *227*(7), 3465–3485. https://doi.org/10.1016/j.jcp.2007.01.037

Smith, R. (1979). The influence of the Earth's rotation on mountain wave drag. *Journal of the Atmospheric Sciences*, *36*(1), 177–180. https://doi.org/10.1175/1520-0469(1979)036<0177:TIOTER>2.0.CO;2

Steyn, D. G., De Wekker, S. F. J., Kossmann, M., & Martilli, A. (2013). Boundary layers and air quality in mountainous terrain. In F. K. Chow, S. F. J. De Wekker, & B. J. Snyder (Eds.), *Mountain Weather Research and Forecasting: Recent Progress and Current Challenges* (pp. 261–289). Springer.

Stockwell, W. R., Kirchner, F., Kuhn, M., & Seefeld, S. (1997). A new mechanism for regional atmospheric chemistry modeling. *Journal of Geophysical Research*, *102*(D22), 25847–25879. https://doi.org/10.1029/97jd00849

Stull, R. B. (1988). *An introduction to boundary layer meteorology*. Springer Netherlands.

Tang, Y., Tong, D. Q., Yang, K., Lee, P., Baker, B., Crawford, A., et al. (2020). Air quality impacts of the 2018 Mt. Kilauea Volcano eruption in Hawaii: A regional chemical transport model study with satellite-constrained emissions. *Atmospheric Environment*, *237*, 117648. https://doi.org/10.1016/j.atmosenv.2020.117648

Tett, S. F. B., Stott, P. A., Allen, M. R., Ingram, W. J., & Mitchell, J. F. B. (1999). Causes of twentieth-century temperature change near the Earth's surface. *Nature*, *399*(6736), 569–572. https://doi.org/10.1038/21164

Theys, N., Romahn, F., & Wagner, T. (2022). S5P mission performance centre sulphur dioxide [L2_SO2_] readme. Retrieved from https://sentinels.copernicus.eu/documents/d/sentinel/s5p-mpc-bira-prf-so2_v02-06-01_2-8_20231129_signed

Thomas, M. A., Brännström, N., Persson, C., Grahn, H., von Schoenberg, P., & Robertson, L. (2017). Surface air quality implications of volcanic injection heights. *Atmospheric Environment*, *166*, 510–518. https://doi.org/10.1016/j.atmosenv.2017.07.045

Tong, N. Y. O., Leung, D. Y. C., & Liu, C.-H. (2011). A review on ozone evolution and its relationship with boundary layer characteristics in urban environments. *Water, Air, & Soil Pollution*, *214*(1), 13–36. https://doi.org/10.1007/s11270-010-0438-5

Torres, F. G., & De-la-Torre, G. E. (2022). Mercury pollution in Peru: Geographic distribution, health hazards, and sustainable removal technologies. *Environmental Science and Pollution Research*, *29*(36), 54045–54059. https://doi.org/10.1007/s11356-022-21152-7

Valdivia-Silva, J. E., Navarro-González, R., & McKay, C. (2009). Thermally evolved gas analysis (TEGA) of hyperarid soils doped with microorganisms from the Atacama Desert in southern Peru: Implications for the Phoenix mission. *Advances in Space Research*, *44*(2), 254–266. https://doi.org/10.1016/j.asr.2009.02.008

Vasquez-Apestegui, B. V., Parras-Garrido, E., Tapia, V., Paz-Aparicio, V. M., Rojas, J. P., Sanchez-Ccoyllo, O. R., & Gonzales, G. F. (2021). Association between air pollution in Lima and the high incidence of COVID-19: Findings from a post hoc analysis. *BMC Public Health*, *21*(1), 1161. https://doi.org/10.1186/s12889-021-11232-7

von Glasow, R., Bobrowski, N., & Kern, C. (2009). The effects of volcanic eruptions on atmospheric chemistry. *Chemical Geology*, *263*(1), 131–142. https://doi.org/10.1016/j.chemgeo.2008.08.020

Whitty, R. C. W., Ilyinskaya, E., Mason, E., Wieser, P. E., Liu, E. J., Schmidt, A., et al. (2020). Spatial and temporal variations in SO_2 and $PM_{2.5}$ levels around Kīlauea Volcano, Hawai'i During 2007–2018. *Frontiers in Earth Science*, *8*. https://doi.org/10.3389/feart.2020.00036

Xue, M., Droegemeier, K. K., & Wong, V. (2000). The Advanced Regional Prediction System (ARPS)—A multiscale nonhydrostatic atmospheric simulation and prediction tool. Part I: Model dynamics and verification. *Meteorology and Atmospheric Physics*, *75*(3–4), 161–193. https://doi.org/10.1007/s007030070003

Xue, M., Droegemeier, K. K., Wong, V., Shapiro, A., Brewster, K., Carr, F., et al. (2001). The Advanced Regional Prediction System (ARPS)—A multi-scale nonhydrostatic atmospheric simulation and prediction tool. Part II: Model physics and applications. *Meteorology and Atmospheric Physics*, *76*(1–4), 143–165. https://doi.org/10.1007/s007030170027

Xue, M., & Thorpe, A. J. (1991). A mesoscale numerical model using the nonhydrostatic pressure-based sigma-coordinate equations: Model experiments with dry mountain flows. *Monthly Weather Review*, *119*(5), 1168–1185. https://doi.org/10.1175/1520-0493(1991)119<1168:AMNMUT>2.0.CO;2

Xue, M., Wang, D., Gao, J., Brewster, K., & Droegemeier, K. K. (2003). The Advanced Regional Prediction System (ARPS), storm-scale numerical weather prediction and data assimilation. *Meteorology and Atmospheric Physics*, *82*(1–4), 139–170. https://doi.org/10.1007/s00703-001-0595-6

Yamasoe, M. A., Sauvage, B., Thouret, V., Nédélec, P., Flochmoen, E. L., & Barret, B. (2015). Analysis of tropospheric ozone and carbon monoxide profiles over South America based on MOZAIC/IAGOS database and model simulations. *Tellus B: Chemical and Physical Meteorology*, *67*(1), 27884. https://doi.org/10.3402/tellusb.v67.27884

Yorks, J. E., Thompson, A. M., Joseph, E., & Miller, S. K. (2009). The variability of free tropospheric ozone over Beltsville, Maryland (39N, 77W) in the summers 2004–2007. *Atmospheric Environment*, *43*(11), 1827–1838. https://doi.org/10.1016/j.atmosenv.2008.12.049

Zardi, D., & Whiteman, C. D. (2013). Diurnal mountain wind systems. In F. K. Chow, S. F. J. De Wekker, & B. J. Snyder (Eds.), *Mountain Weather Research and Forecasting: Recent Progress and Current Challenges* (pp. 35–119). Springer.

Zhang, J., & Rao, S. T. (1999). The role of vertical mixing in the temporal evolution of ground-level ozone concentrations. *Journal of Applied Meteorology*, *38*(12), 1674–1691. https://doi.org/10.1175/1520-0450(1999)038<1674:TROVMI>2.0.CO;2

Zhang, J., Rao, S. T., & Daggupaty, S. M. (1998). Meteorological processes and ozone exceedances in the northeastern United States during the 12-16 July 1995 Episode*. *Journal of Applied Meteorology*, *37*(8), 776–789. https://doi.org/10.1175/1520-0450(1998)037<0776:mpaoei>2.0.co;2

Zhang, L., Guo, X., Zhao, T., Gong, S., Xu, X., Li, Y., et al. (2019). A modelling study of the terrain effects on haze pollution in the Sichuan Basin. *Atmospheric Environment*, *196*, 77–85. https://doi.org/10.1016/j.atmosenv.2018.10.007

Zhang, Z., Xu, X., Qiao, L., Gong, D., Kim, S.-J., Wang, Y., & Mao, R. (2018). Numerical simulations of the effects of regional topography on haze pollution in Beijing. *Scientific Reports*, *8*(1), 5504. https://doi.org/10.1038/s41598-018-23880-8